Article

Methane Conversion to Ethylene and Aromatics on PtSn Catalysts

Duygu Gerceker, Ali Hussain Motagamwala, Keishla R. Rivera-Dones, James B. Miller, George W. Huber, Manos Mavrikakis, and James A. Dumesic

ACS Catal., **Just Accepted Manuscript** • Publication Date (Web): 03 Feb 2017

ACS Catalysis is published by the American Chemical Society. 1155 Sixteenth Street N.W., Washington, DC 20036

Methane Conversion to Ethylene and Aromatics on PtSn Catalysts

*Duygu Gerceker[a], Ali Hussain Motagamwala[a,b], Keishla R. Rivera-Dones[a], James B. Miller[a], George W. Huber[a], Manos Mavrikakis[a], James A. Dumesic[a]**

[a] Department of Chemical and Biological Engineering, University of Wisconsin-Madison, Madison, Wisconsin 53706, USA

[b] Great Lakes Bioenergy Research Center, University of Wisconsin-Madison, 1552 University Ave., Madison, WI 53726, USA

Abstract: Pt and PtSn catalysts supported on SiO_2 and H-ZSM-5 were studied for methane conversion under non-oxidative conditions. Addition of Sn to Pt/SiO_2 increased the turnover frequency for production of ethylene by a factor of 3, and pretreatment of the catalyst at 1123 K reduced the extent of coke formation. Pt and Pt-Sn catalysts supported on H-ZSM-5 zeolite were prepared to improve the activity and selectivity to non-coke products. Ethylene formation rates were 20 times faster over a Pt-Sn(1:3)/H-ZSM-5 catalyst with SiO_2:Al_2O_3 = 280, than over Pt-Sn(3:1)/SiO_2. H-ZSM-5 supported catalysts were also active for the formation of aromatics, and the rates of benzene and naphthalene formation were increased by using more acidic H-ZSM-5 supports. These catalysts operate through a bifunctional mechanism, in which ethylene is first produced on highly dispersed PtSn nanoparticles, and then is subsequently converted to benzene and naphthalene on Brønsted acid sites within the zeolite support. The most active and stable PtSn catalyst forms carbon products at a rate, 2.5 mmol-C/mol-Pt.s, that is comparable to that of state-of-the-art Mo/H-ZSM-5 catalysts with same metal loading and operated under similar conditions (1.8 mmol-C/mol-Mo.s). Scanning transmission electron microscopy measurements suggest the presence of smaller Pt nanoparticles on H-ZSM-5 supported catalysts, compared to SiO_2-supported catalysts, as a possible source of their high activity. A microkinetic model of methane conversion on Pt and PtSn surfaces, built using results from density functional theory calculations, predicts higher coupling rates on bimetallic and stepped surfaces, supporting the experimental observations that relate the high catalytic activity to small PtSn particles.

Keywords: methane conversion**,** platinum, tin, H-ZSM-5, ethylene, aromatics, microkinetic model, particle size

1. Introduction

Methane is a stable molecule that is difficult to activate without significant energy input.[1] The goal of activating methane and converting it into more valuable chemicals has long been recognized as an important challenge.[2] Many studies have addressed oxidative coupling of methane, usually over catalysts that are composed of or modified by alkali and alkali earth metal compounds.[1] As an alternative approach, dehydroaromatization (DHA), a non-oxidative coupling of methane to ethane, ethylene and aromatics, has received significant attention. However, thermodynamic considerations limit methane conversion of dehydroaromatization to less than 10% for C_2 products, even at high temperatures (970 K), while formation of carbon is highly favored.[2] Accumulation of carbon on the catalyst surface results in deactivation and loss of selectivity. A promising class of catalysts for methane dehydroaromatization is comprised of shape selective silica-alumina zeolites, such as ZSM-5, ZSM-8, ZSM-11 and MCM-22 modified with transition metal species, such as Mo.[3, 4, 5]

Early work by Wang, et al. reported that benzene could be produced on Mo or Zn modified ZSM-5 catalysts at 973 K under non-oxidizing conditions.[6] A bifunctional mechanism was proposed, with activation of methane on molybdenum containing sites, dimerization of CH_3 radicals to form ethane and the primary product ethylene, followed by aromatization of ethylene to benzene on Brønsted acid sites.[7,8] The presence of Mo_2C was found to be necessary for the formation of hydrocarbons.[8,9,10] Furthermore, partial oxidation of Mo_2C resulted in higher hydrocarbon formation rates, suggesting that Mo_2C-MoO_2 with an oxygen deficiency provided the active catalytic sites for methane activation.[11] Pretreatment of Mo/H-ZSM-5 with an n-butane/hydrogen mixture formed β-Mo_2C and α-MoC_{1-x} species that were responsible for the higher production rate of aromatic compounds and slower deactivation of the catalyst.[12] A reaction mechanism involving the formation of acetylene as an important reaction intermediate was suggested.[13]

Various modifications in the reaction conditions and catalyst formulation for Mo/H-ZSM-5 have been studied to improve catalytic activity and minimize deactivation due to coke formation. Co-feeding with H_2 shifted the equilibrium back toward methane, resulting in both decreased coke deposition and lower hydrocarbon formation rates.[14] Modification of Mo/H-ZSM-5 with Rh provided a catalyst that was stable when operated at 1023 K with a 6% H_2/CH_4 feed. Rh was proposed to suppress the coke formation on Brønsted acid sites, thereby enhancing catalyst stability.[15] Co-feeding of up to 5% CO_2 was found to result in lower coke formation rates on

Mo/H-ZSM-5 and Fe or Co modified Mo/H-ZSM-5.[16, 17] High pressures of CO_2 were observed to oxidize the Mo_2C formed during the induction period, resulting in lower catalytic activity.[18]

Under cyclic operation between CH_4 and H_2 flows, addition of Fe to Mo/H-ZSM-5 improved catalyst stability through formation of carbon nanotubes with H_2 release under CH_4 flow. The carbon nanotubes were subsequently removed by flowing H_2, regenerating the active sites. The cyclic evolution of H_2 provided decreased coke formation.[19] In a recent study of the effect of Co addition in the range of 0-1.6%, a Mo/H-ZSM-5 catalyst containing 0.8 wt% Co showed optimal performance for benzene formation and favored formation of heavier products.[20] The effects of Ga[21], Zr[22], W[23] and Ru modification of Mo/H-ZSM-5 system were also investigated to achieve more stable and active catalysts with decreased coke formation.[24,25]

The structures and locations of the carbonaceous deposits that lead to deactivation of Mo/H-ZSM-5 have been examined to gain insight about their interactions with methane and formation of intermediates during reaction. XPS characterization of spent Mo/H-ZSM-5 samples revealed three types of carbon species on the spent catalyst: the first type is a graphitic-like carbon present in the zeolite channels; the second type is carbidic-like carbon in Mo_2C mainly located at the outer surface of the zeolite; and the third type is hydrogen-poor pre-graphitic type, the quantity of which increased with time on stream. Located on the outer portions of the zeolite, the third carbon type was thought to be responsible for deactivation of the catalyst.[26] In another study, it was shown that some of the carbon species deposited on the surface were reactive and could be hydrogenated to yield ethylene and benzene at 839 K and 913 K, respectively.[27] In a recent study, three stages of Mo-H-ZSM-5 deactivation were identified. The first stage was rapid deactivation due to carburization of MoO_3 to Mo_2C accompanied by carbon deposition on the external surface of the catalyst. The second stage exhibited slower deactivation due to coke being deposited in the micropores of the support during benzene and naphthalene formation. A third deactivation period was characterized by a sharp decrease in aromatics formation, attributed to the blocking of the channels with carbon deposits near the pore mouths.[28]

In addition to studies that investigated the activity of various transition metals such as Fe, Re, V and Cr supported on SiO_2 and H-ZSM-5, methane conversion has also been studied on Pt-containing catalysts.[29,30,31,32] In an early work that addressed low temperature activation of methane, a 6 wt% Pt/SiO_2 catalyst was first exposed to methane at 523 K and then flushed with H_2, resulting in the formation of hydrocarbon products ranging from C_2 to C_7. Pt/HX and Pt/HY catalysts with the same Pt loading exhibited higher methane conversion and higher formation rates of C_3 and C_5 products. The catalysts were not effective at higher temperatures because of coke deposition on Pt.[33,34] At 973 K, a 2 wt% Pt/H-ZSM-5 catalyst exhibited low methane conversions. However, adding Pt to Mo/H-ZSM-5 improved the catalytic activity of Mo/H-ZSM-5 by decreasing the rate of coke formation.[35,36] The active sites of the catalyst were hypothesized to be associated with a Pt-MoO_3-H-ZSM-5 structure on the catalyst.[37] At 973 K, addition of 0.1 wt% Sn to the Pt-Mo/H-ZSM-5 catalyst yielded slightly lower methane conversion while decreasing the extent of coke deposition and increasing the selectivity to aromatics. Catalysts prepared by sequential impregnation of Pt followed by Sn exhibited higher benzene selectivity and better coke mitigation compared to catalysts prepared by co-impregnation.[38, 39]

In this work, we present a study of non-oxidative methane conversion on Pt-Sn bimetallic catalysts that exhibit high activity, selectivity, and stability for production of ethylene. We also show that the addition of Brønsted acid sites to Pt-Sn/ZSM-5 leads to catalysts that are active for the conversion of methane to benzene and naphthalene, through a bifunctional mechanism, whereby ethylene is produced on highly dispersed PtSn nanoparticles, followed by its conversion to benzene and naphthalene on Brønsted acid sites within the zeolite support. A microkinetic model built using results from density functional theory calculations (DFT) for terrace and step sites of Pt and PtSn surfaces predicts higher rates of ethylene formation on bimetallic step sites.

2. Experimental

Catalyst preparation: Catalysts consisting of Pt and Pt-Sn supported on SiO_2 and H-ZSM-5 were prepared by impregnation. For SiO_2-supported catalysts, Davisil (Grade 646, 35-60 mesh, Sigma Aldrich) was impregnated with an aqueous solution of tetraammine platinum (II) nitrate precursor (Sigma Aldrich, 99%) to the target loading of 6 wt% Pt. After drying overnight at 373 K, the catalyst was calcined under air flow (50 cm^3(STP)/min) at 573 K for 2 h, followed by reduction in flowing hydrogen (50 cm^3(STP)/min) at 773 K for 2 h. Prior to contacting with air, the catalyst was cooled to room temperature under Ar flow and passivated with flowing 1% O_2/Ar for 30 min. Addition of Sn to Pt/SiO_2 was performed through evaporative impregnation. To achieve an overall atomic ratio of Pt/Sn equal to 3:1, the required amount of the Sn precursor, tri-n-butyl tin (Strem Chemicals Inc, min 94%), was dissolved in 80 mL n-pentane (Sigma Aldrich), stirred for 5 min and then Pt/SiO_2 was added. The mixture was stirred until all the pentane had evaporated, and the catalyst was then dried for 30 min in an oven at 373 K. Calcination, reduction and passivation steps were repeated for the resulting catalyst. Catalysts prepared via this procedure were labeled as Pt/SiO_2 and PtSn/SiO_2. For zeolite-supported catalysts, four different ZSM-5 supports with nominal SiO_2/Al_2O_3 ratios of 23, 50, 80 and 280 were obtained in NH_4^+ form (Zeolyst). Prior to impregnation, supports were calcined in air at 873 K for 18 h to remove ammonia and obtain the H-ZSM-5 form. Based on the targeted Pt-Sn atomic ratio for a 0.58 wt% Pt catalyst, the required amount of the Sn precursor was dissolved in methanol and impregnated onto the zeolite support. After drying overnight at 373 K, the catalyst was calcined under air flow (50 cm^3(STP)/min) at 573 K for 2 h. Subsequently, Sn/H-ZSM-5 was impregnated with Pt using an aqueous solution of tetraammine platinum (II) nitrate precursor. The resulting catalyst was dried overnight at 373 K, treated in Ar (50 cm^3(STP)/min) at 573 K for 1 h, and reduced at 773 K for 6 h. Prior to contacting with air, the catalyst was cooled to room temperature under Ar flow and passivated with flowing 1% O_2/Ar for 30 min. Catalysts prepared by this procedure were labeled as Pt/Z-280, PtSn(1:1)/Z-280, PtSn(1:2)/Z-280, PtSn(1:2.5)/Z-280, PtSn(1:3)/Z-280, PtSn(1:2)/Z-80, PtSn(1:2)/Z-50 and PtSn(1:2)/Z-23 based on their composition and SiO_2/Al_2O_3 ratio. For zeolite supported samples, higher Sn content was targeted to overcome the possible interaction of Sn with alumina sites.[40]

Catalyst characterization: Platinum surface site densities of the fresh catalysts were determined by CO chemisorption at 308 K (Micromeritics, ASAP, 2020C Analyzer). Turnover frequencies (TOF) for product formation were normalized by the Pt site density value of the catalyst.

Textural properties of the blank and impregnated H-ZSM-5 catalysts were determined from N_2 adsorption-desorption isotherms obtained at 77 K using the same instrument. Prior to the adsorption measurements, samples were degassed at 423 K and evacuated for 6 h. Specific surface areas of the catalysts were calculated by the BET method.

The acid site densities of fresh and spent catalysts were measured by NH_3–temperature programmed desorption (NH_3-TPD). 100 mg of each catalyst sample was heated to 473 K under helium flow and kept at constant temperature for 1 h. After cooling to 423 K, NH_3 was adsorbed on the sample from a 1% NH_3/He flow for 45 min. Following a purge with helium at 423 K for

90 min to remove weakly adsorbed NH_3, the sample was heated to 973 K under helium flow with a 10 K/min ramp and held at 973 K for 2 h.

Thermogravimetric analysis (TGA) was performed on spent catalysts to quantify the amount of deposited coke (TGA 500). In this analysis, 25-30 mg of the spent catalyst sample was heated from room temperature to 973 K with a ramp of 20 K/min under oxygen flow. The change in the sample mass due to combustion of coke and release of CO_2 was used in the calculation of the amount of coke deposition.

Scanning transmission electron microscopy (STEM) imaging was performed using a FEI Titan STEM with Cs aberration correction operated at 200 kV in high-angle annular dark field (HAADF) mode. Catalyst samples were suspended in ethanol then deposited on a holey carbon Cu TEM grid. Samples were plasma cleaned before being loaded into the microscope. ImageJ software was used to analyze the micrographs and to calculate particle size distributions.

Methods: Reaction kinetics experiments were conducted in a ½ - inch stainless steel down flow reactor. The required mass of catalyst (2 g for SiO_2 supported catalysts, 1 g for zeolite supported catalysts) was loaded in the reactor in three sections separated with quartz wool to minimize channeling. Following the reduction with H_2 for 1 h at 773 K, the catalyst was heated to 973 K under flowing He, and then 42 cm^3(STP)/min CH_4 flow was introduced as feed. For the experiments comparing the effect of support acidity, 0.25 g catalyst was packed with 2-2.5 g of silica chips for each experiment, and the CH_4 flowrate was decreased to 10.5 cm^3(STP)/min. For certain runs with the SiO_2-supported catalysts, the catalysts were further reduced at 1123 K for 2 h prior to the reaction. For experiments with H_2 co-feeding, H_2 gas corresponding to 5% of the CH_4 flow was introduced from a 10% H_2/He tank (Airgas). Analysis of the products, except naphthalene, was carried out by an online gas chromatograph (Shimadzu Corp., GC-2014) equipped with a Rt®-Alumina BOND/MAPD capillary column and a flame ionization detector. To detect naphthalene, the same gas chromatograph equipped with an Agilent J&W GS-GasPro column was used. All the lines between reactor outlet and GC sampling loop inlet were heat traced to 493 K to prevent product condensation.

3. Results and Discussion

3.1. Catalyst Characterization:

CO chemisorption: The platinum surface site densities of the catalysts determined by CO chemisorption are shown in Table 1. Because all the catalysts were initially reduced at 773 K during catalyst preparation, the CO uptakes of the fresh catalysts were measured following an in situ reduction at 773 K. On both supports, compared to monometallic Pt catalysts, the presence of Sn decreased the number of Pt sites accessible for CO chemisorption, suggesting that formation of bimetallic particles took place. To identify the effect of treatment at high temperatures, samples of Pt/SiO_2 and PtSn/SiO_2 catalysts were reduced at 1123 K, and samples of Pt/Z-280 and PtSn(1:3)/Z-280 were reduced at 973 K, prior to CO chemisorption measurements. The number of surface Pt sites on the Pt/SiO_2 catalyst decreased by 75% after treatment at 1123 K, and surface site density on PtSn/SiO_2 decreased only by 55%, suggesting that the presence of Sn decreased the extent of sintering. The number of surface Pt sites on Pt/Z-280 and PtSn(1:3)/Z-280 decreased by approximately 50% after treatment at 973 K.

Table 1. Platinum surface site densities of catalysts determined by CO chemisorption

Catalyst	Pretreatment Temperature (K)	Site density (μmol Pt/g)	Catalyst	Pretreatment Temperature (K)	Site density (μmol Pt/g)
Pt/SiO_2[#]	773	76	Pt/SiO_2[#]	1123	19
$PtSn/SiO_2$[#,a]	773	30	$PtSn/SiO_2$[#,a]	1123	13
Pt/Z-280	773	7.5	Pt/Z-280	973	3.4
PtSn(1:1)/Z-280	773	6.6	PtSn(1:2)/Z-280	773	5.6
PtSn(1:2)/Z-80	773	6.3	PtSn(1:2)/Z-50	773	4.8
PtSn(1:2)/Z-23	773	8.9	PtSn(1:2.5)/Z-280	773	4.9
PtSn(1:3)/Z-280	773	3.7	PtSn(1:3)/Z-280	973	1.8

[#]SiO_2 supported catalysts had Pt loading of 6 wt% and zeolite supported catalysts had Pt loading of 0.58 wt%.
[a] $PtSn/SiO_2$ catalysts have an overall atomic ratio of Pt/Sn equal to 3:1

Surface area characterization: N_2 physisorption was employed to obtain surface areas of the blank supports and metal impregnated supports with varying acidity. BET surface areas of the blank H-ZSM-5 supports were in agreement with values reported in the literature.[6,41] As shown in Table 2, catalysts impregnated with only-Sn and with Sn followed by Pt, had lower BET surface areas than the blank supports. This decrease suggests that the impregnated metals entered the pores of the support. The BET surface area of a spent PtSn(1:3)/Z-280 catalyst sample yielded an even lower BET surface area, probably due blockage of the pores by carbonaceous deposits formed during methane conversion reactions.

Table 2. BET surface areas of supports and catalysts measured by N_2 physisorption*

Support	BET surface area (m^2/g)	Catalyst	BET surface area (m^2/g)
Z-23	355	Pt/Z-280	384
Z-50	397	Sn/Z-280	342
Z-80	351	PtSn(1:3)/Z-280	333
Z-280	378	PtSn(1:3)/Z-280-spent	306

(* +/- 5 m^2/g)

NH_3-Temperature Programmed Desorption: The acid site densities of the blank supports, the impregnated catalysts, and the spent samples are shown in Table 3**.** As expected, the calculated acid site density from the desorption of ammonia decreased with increasing SiO_2:Al_2O_3 ratio of the H-ZSM-5 support (from 850 μmol/g to 62 μmol/g). The same trend was observed with the samples of fresh catalysts on which Sn and Pt were impregnated (from 710 μmol/g to 41 μmol/g). Similarly, on the spent catalysts collected at the end of the reaction, the acid site density decreased with increasing SiO_2:Al_2O_3 ratio; however, the range of the values was narrower (from 140 μmol/g to 90 μmol/g). This difference may be related to the accumulation of coke deposits on the acid sites of the support.

Table 3. Acid site density of supports and catalysts determined by NH_3-TPD

Support	Acid site density (μmol/g)	Catalyst (fresh)	Acid site density (μmol/g)	Catalyst (spent)	Acid site density (μmol/g)
Z-23	850	PtSn(1:2)/Z-23	710	PtSn(1:2)/Z-23	140
Z-50	270	PtSn(1:2)/Z-50	280	PtSn(1:2)/Z-50	120
Z-80	250	PtSn(1:2)/Z-80	250	PtSn(1:2)/Z-80	120
Z-280	62	PtSn(1:2)/Z-280	41	PtSn(1:2)/Z-280	90

3.2. Effect of pretreatment temperature on SiO_2 supported catalysts:

Pt/SiO_2 and bimetallic PtSn/SiO_2 catalysts, pretreated at 773 and 1123 K, were studied for coke formation trends under reaction conditions both with and without 5% H_2 co-feeding. It was observed that catalysts pretreated at 773 K had carbon balances as low as 65% during the initial period of reaction (e.g., 0.5 h) due to coke deposition. Pretreatment at 1123 K was performed to decrease the surface concentration of silanol groups on the silica surface, in an attempt to minimize the extent of coke formation and to improve the carbon balance. Spent catalysts were collected at the end of 6 h time on stream for each reaction, and thermogravimetric analyses (TGA) were carried out. In parallel, the difference between the inlet and outlet moles of carbon flow of each catalyst integrated over the same time on stream period of 6 h was used to obtain an estimate for the extent of carbon deposition on the catalyst. The calculated amounts of deposited carbon (from TGA analysis after reaction) and carbon loss (from comparison of carbon flow rates into and out of the reactor versus time on stream) for SiO_2-supported catalysts are shown in Table 4.

Table 4. Carbon deposition and calculated carbon loss for SiO_2-supported catalysts

Catalyst	Pretreatment at 773 K		Pretreatment at 1123 K	
	Carbon deposition (TGA) (mmol/gcat)	Carbon loss (mmol/gcat)	Carbon deposition (TGA) (mmol/gcat)	Carbon loss (mmol/gcat)
Pt/SiO_2	14	15	6.7	6.0
Pt/SiO_2 – 5%H_2	13	14	3.6	11
$PtSn/SiO_2$[#]	12	21	5.1	6.1
$PtSn/SiO_2$ – 5%H_2[#]	4.1	7.7	1.8	4.5

[#] $PtSn/SiO_2$ catalysts had overall atomic ratio of Pt/Sn equal to 3:1

As seen from carbon deposition measurements and the calculated carbon losses in each experiment, catalysts pretreated at 1123 K had lower coke deposition as measured by TGA and had higher closure of the carbon balance. As the calculated carbon losses were found to be higher in amount than the carbon detected on the spent catalyst samples in TGA analyses, it is likely that some undetected carbon was deposited on the reactor walls or elsewhere in the reactor system. Hydrogen co-feeding decreased the extent of coke formation, particularly on the $PtSn/SiO_2$ catalyst. When the catalyst was pretreated at 773 K, addition of 5% H_2 resulted in 60% decrease in coke deposition.

3.3. Effect of Sn addition on catalytic activity of SiO_2 supported catalysts: Figure 1a compares the TOF values for ethylene formation as a function of time on stream for the Pt/SiO_2 and bimetallic $PtSn(3:1)/SiO_2$ catalysts pretreated at 1123 K. Addition of Sn to Pt/SiO_2 increased the ethylene TOF, and after five hours on stream, when ethylene TOF achieved a steady value, the $PtSn/SiO_2$ catalyst had approximately 3 times higher ethylene TOF than

Pt/SiO_2. Figure 1b shows the same comparison for the benzene TOF. The PtSn/SiO_2 catalyst pretreated at 1123 K yielded a benzene TOF of 8.6 x 10^{-3} ks^{-1} at the end of five hours on stream, which was approximately 2% of its ethylene TOF. Addition of Sn to Pt/SiO_2 increased the initial benzene activity, and the steady state benzene TOF over PtSn/SiO_2 was approximately 2 times higher than Pt/SiO_2. Figure 1c and Figure 1d display the methane conversion to detectable products (left axis) and the selectivities of the catalyst towards ethylene, ethane and benzene (right axis) over total hydrocarbon products excluding coke for Pt/SiO_2 and PtSn/SiO_2, respectively. The PtSn/SiO_2 catalyst yielded higher methane conversion to products and higher selectivity towards ethylene compared to Pt/SiO_2. Also, both catalysts showed low selectivity towards ethane and benzene.

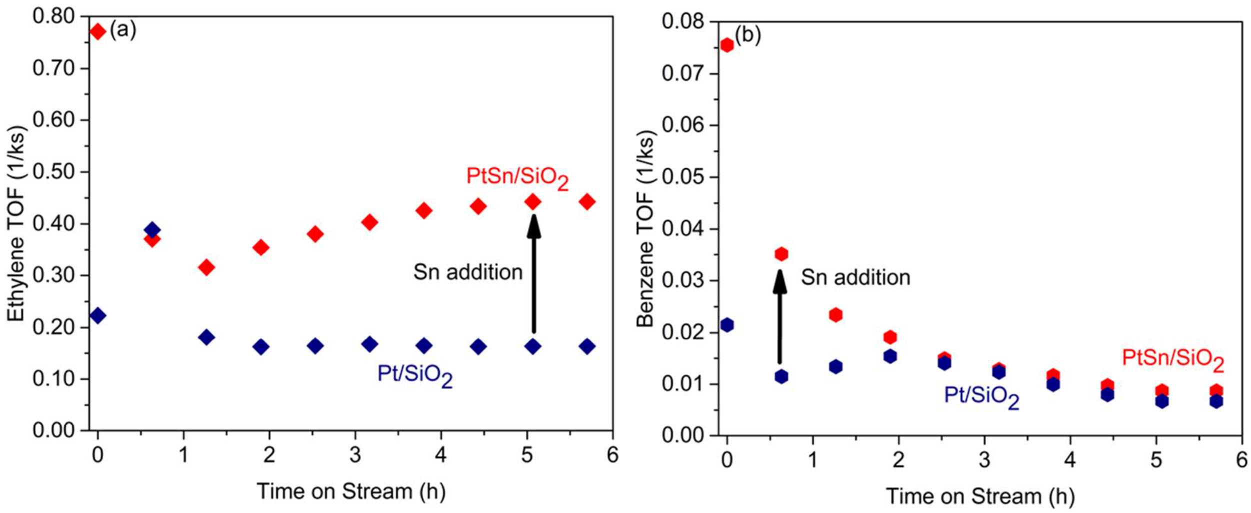

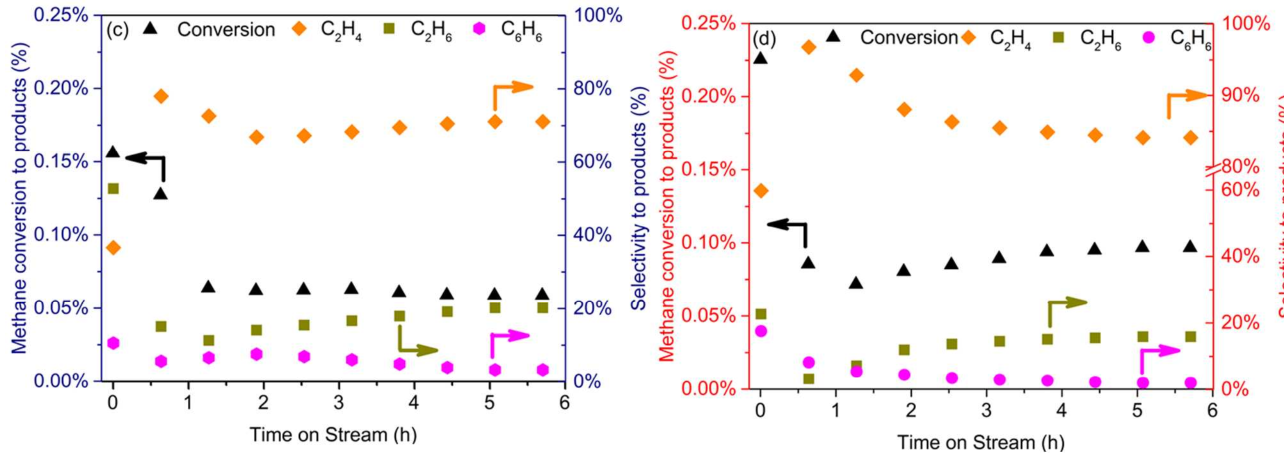

Figure 1. Effect of Sn addition on Pt/SiO_2 pretreated at 1123 K. (a) Ethylene TOF and (b) benzene TOF over Pt/SiO_2 and $PtSn/SiO_2$, methane conversion to detectable products and product selectivities excluding coke for (c) Pt/SiO_2 and (d) $PtSn/SiO_2$. (overall atomic ratio of Pt/Sn equal to 3:1) *Conditions:* CH_4 flowrate = 42 cm^3(STP)/min, T = 973 K, catalyst mass = 2 g.

3.4. Effect of H_2 co-feeding on catalytic activity of SiO_2 supported catalysts:

Co-feeding hydrogen with methane has been used in the literature to decrease coke formation, although it has resulted in lower product formation rates. Accordingly, 5% H_2 was co-fed with methane on Pt and $PtSn/SiO_2$ catalysts pretreated at 1123 K. Figure 2a and Figure 2b display ethylene TOF values for Pt and $PtSn/SiO_2$ catalysts under no co-feed and 5% H_2 co-feeding conditions. On the Pt/SiO_2 catalyst with 5% H_2 co-feeding, following a short term increase, the activity decreased monotonically, and at the end of 6 h, it was 60% of the activity of the catalyst with only methane feed. On the $PtSn/SiO_2$ catalyst, the ethylene TOF decreased monotonically, and the value at steady state with 5% H_2 co-feeding was three times lower than for the catalyst with no co-feeding. As shown in Figure 2c and Figure 2d, the benzene TOF values of the catalysts showed a similar trend; however, the decrease in the TOF due to H_2 co-feeding was more pronounced for the initial period of the time on stream. Methane conversion to detectable products (left axis) and the selectivities of the catalyst towards ethylene, ethane and benzene (right axis) over total hydrocarbon products excluding coke for Pt/SiO_2 and PtSn/SiO_2 with 5% H_2 co-feeding are plotted in Figure 2e and Figure 2f. As indicated by the decreased product TOF values, both catalysts had lower methane conversion when H_2 is co-fed with methane. This trend is in accordance with results from previous studies.

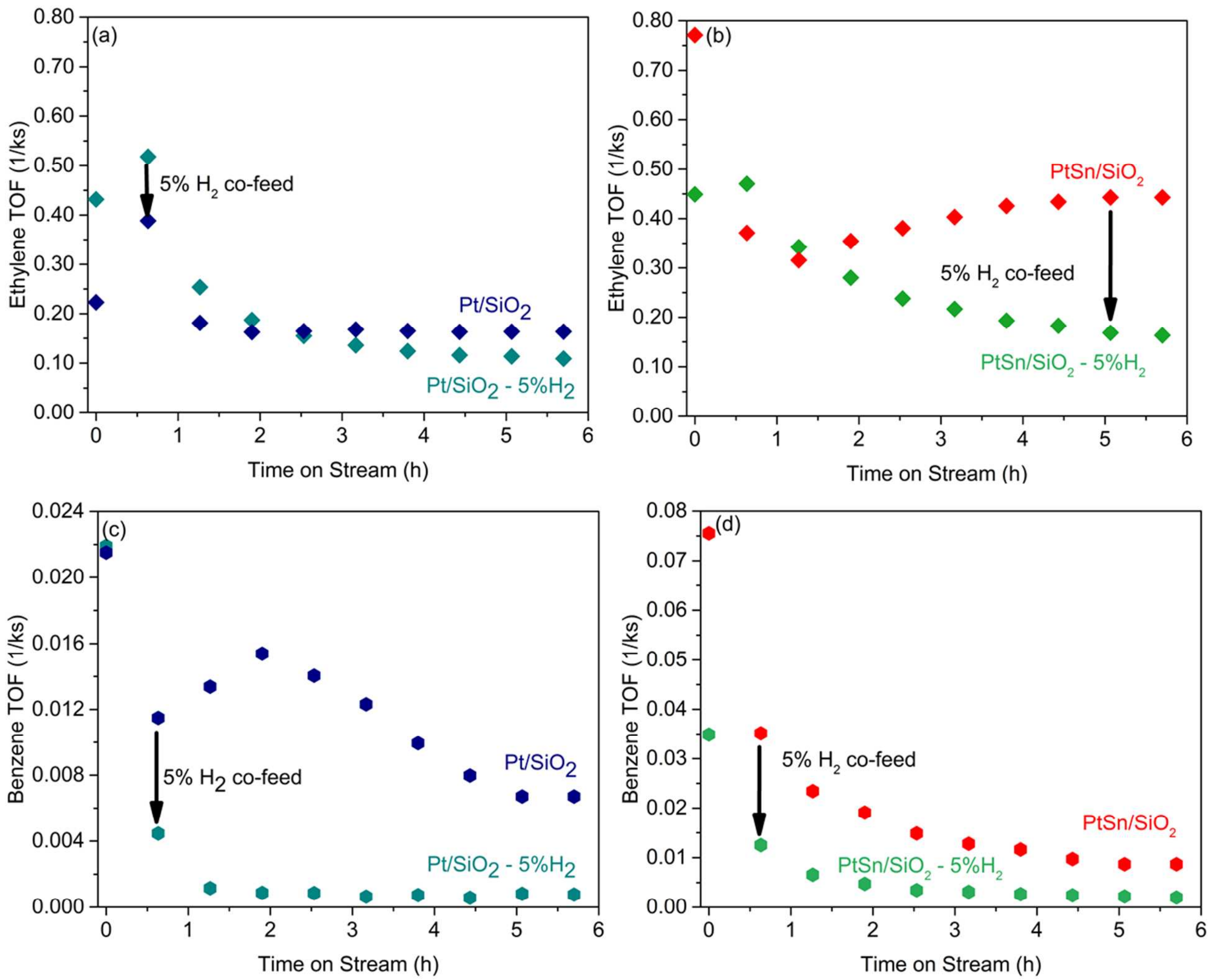

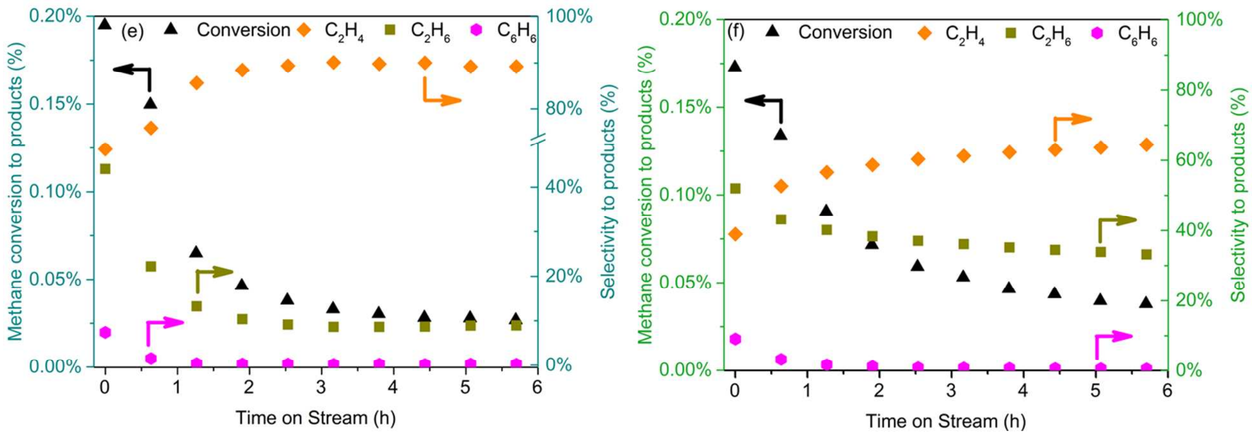

Figure 2. Effect of H_2 co-feeding with CH_4 on SiO_2-supported catalysts pretreated at 1123 K. Ethylene TOF over (a) Pt/SiO_2 and (b) PtSn/SiO_2, benzene TOF over (c) Pt/SiO_2 and (d) PtSn/SiO_2, methane conversion to detectable products and selectivities excluding coke for (e) Pt/SiO_2 with 5% H_2 co-feeding and (f) PtSn/SiO_2 5% H_2 co-feeding. (overall atomic ratio of Pt/Sn equal to 3:1) *Conditions:* CH_4 flowrate = 42 cm^3(STP)/min, T=973 K, catalyst mass = 2 g. H_2 flowrate = 2 cm^3(STP)/min for the co-feeding runs.

3.5. Effect of support and Pt:Sn ratio on the activity of H-ZSM-5 supported catalysts:

H-ZSM-5 zeolite with SiO_2/Al_2O_3 = 280 was investigated for its performance as a support for Pt and PtSn catalysts. Figure 3a shows the ethylene TOF as a function of time on stream. PtSn(1:1)/Z-280 and PtSn(1:2.5)/Z-280 catalysts were also studied for CH_4 conversion, and they performed similar to PtSn(1:2)/Z-280. These data are omitted here for the sake of clarity. As the Sn content increased, the ethylene TOF of the zeolite-supported catalysts increased. At the end of 6 h, the ethylene TOF on the Pt-Sn(1:3)/Z-280 catalyst was 4 times higher than the ethylene TOF on the Pt/Z-280 catalyst and 15 times faster than that of the PtSn/SiO_2 catalyst. In evaluating the activity of zeolite-supported catalysts for benzene formation, the formation rate of the product per mass of catalyst was used instead of TOF values normalized per Pt site density of the catalyst surface. The rationale behind this choice was the bifunctional nature of these catalysts leading to the formation of aromatic compounds on acid sites of the zeolite. Figure 3b displays the benzene formation rate of Pt and PtSn catalysts supported on H-ZSM-5 per mass of catalyst. The rate of benzene formation was promoted by the zeolite support, as evidenced by the 4 times increase in the benzene formation rate with the use of a bimetallic catalyst Pt-Sn on the zeolite support. A significant difference between the formation of ethylene and benzene was that while the benzene formation rate deactivated within the first two hours, the rate of ethylene formation kept increasing up to 10 h time on stream, particularly on the bimetallic catalysts. Figure 3c and Figure 3d display the methane conversion to detectable products (left axis) and the selectivities of the catalyst towards ethylene, ethane and benzene (right axis) over total hydrocarbon products excluding coke for Pt/Z-280 and Pt-Sn(1:3)/Z-280 catalysts. In parallel with the variation of ethylene TOF profiles of the catalysts, Pt/Z-280 showed a flat conversion profile around 0.05%, while the conversion over Pt-Sn(1:3)/Z-280 exceeded 0.10% at the end of 8 h. Ethylene was the product with highest selectivity on both catalysts, while Pt-Sn(1:3)/Z-280 also yielded a significant benzene selectivity around 10%. The zeolite-supported catalysts performed better than their silica supported counterparts, and bimetallic PtSn catalysts were more active than Pt/Z-280 for formation of both ethylene and benzene.

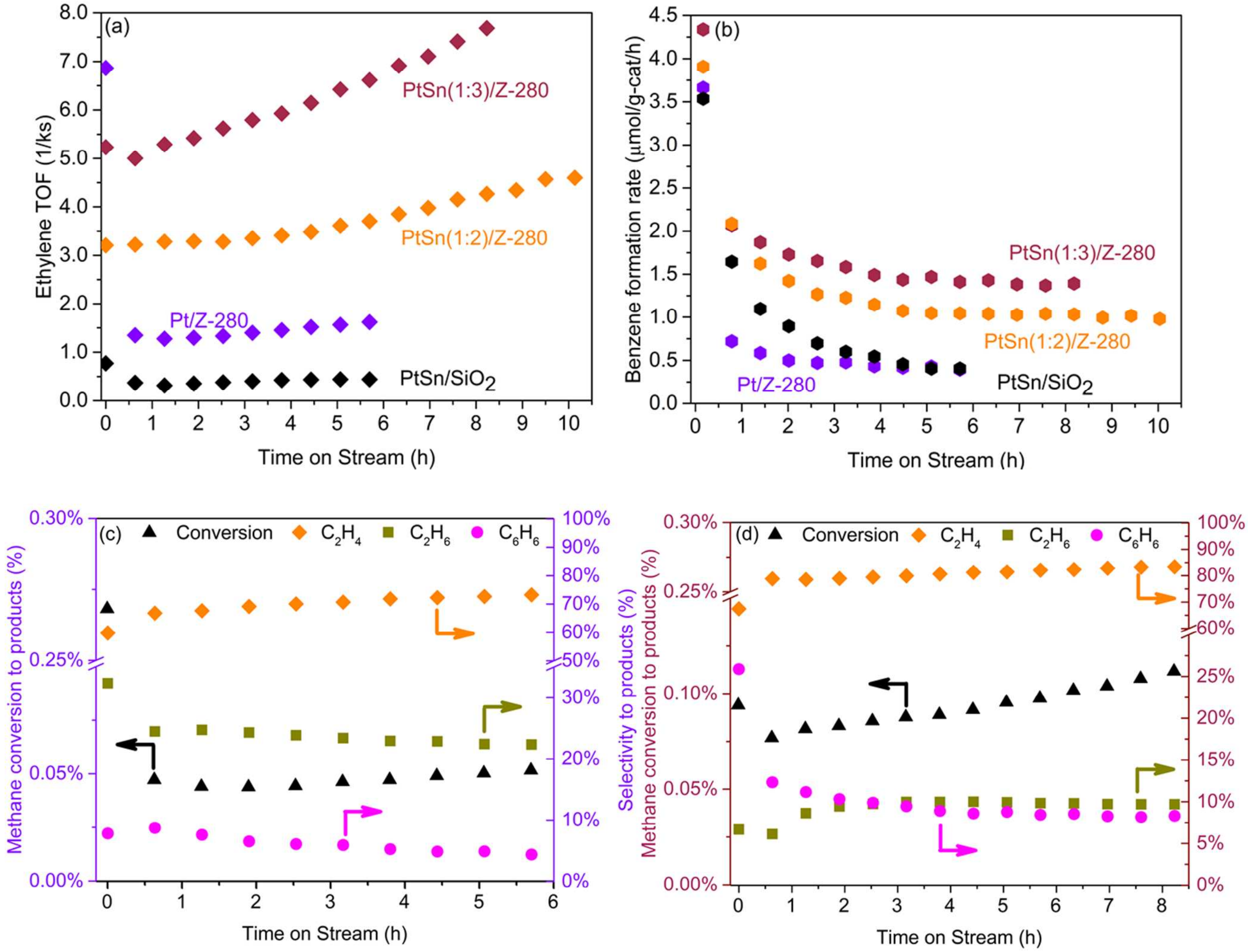

Figure 3. Effect of Sn addition to Pt/Z-280. (a) Ethylene TOF (b) benzene formation rate per mass of catalyst over Pt/Z-280 and PtSn/Z-280, methane conversion to detectable products and selectivities excluding coke for (c) Pt/Z-280 and (d) PtSn(1:3)/Z-280. Ethylene TOF and benzene formation rate over PtSn/SiO_2 (overall atomic ratio of Pt/Sn equal to 3:1) are given for comparison. *Conditions:* CH_4 flowrate = 42 cm^3(STP)/min, T = 973 K, catalyst mass = 1 g.

As explained in more detail below, a microkinetic model based on results from DFT calculations suggests that smaller Pt-Sn particles should be more active for methane conversion.

Thus, it can be hypothesized that PtSn/H-ZSM-5 catalysts have smaller particle sizes compared to SiO_2-supported catalysts. STEM images were collected to obtain information about the particle size distributions of the studied catalysts. Figure 4 displays STEM images of Pt/SiO_2 and Pt/H-ZSM-5 samples. The histograms of the particle size distributions of the two catalysts are shown in Figure 5. The particle size distributions for these catalysts showed that the surface-averaged particle sizes of the Pt/SiO_2 and Pt/Z-280 catalysts were 2.5 nm and 1.8 nm, respectively. The origin of the smaller metal particle size on the H-ZSM-5 catalyst can be attributed to its higher surface area compared to SiO_2 (425 m^2/g for H-ZSM-5 versus 300 m^2/g for SiO_2). As another way to investigate the effect of particle size of the catalyst, the variation of the fraction of total metal surface area was calculated as a function of the metal particle diameter. This variation of the fraction of total metal surface area versus particle size is shown in the inset of Figure 5. Sixty percent of the surface area for the Pt/Z-280 catalyst was in the particle diameter range from 1-2 nm. In contrast, only 15% of the surface area of Pt/SiO_2 was in this same region. To investigate the effect of Sn on the particle size, STEM images were collected for the PtSn/SiO_2 catalyst with overall atomic ratio of Pt/Sn equal to 3:1 and for the PtSn(1:3)/Z-280 catalyst. The average particle size of the PtSn/SiO_2 catalyst was 2.5 nm, while the average particle size of the PtSn(1:3)/Z-280 catalyst was 2.3 nm. EDS analysis of the catalysts showed that the bimetallic particles on the PtSn/SiO_2 catalyst were composed of 4.5 at% Sn, whereas the target value was 25%. The same analysis yielded a composition of 23 at% Sn on the Pt-Sn(1:3)/Z-280 catalysts that had the target atomic fraction of 75 at% Sn. Although both catalysts had lower than expected amounts of Sn interacting with Pt, formation of bimetallic particles was more successful on the zeolite support, as shown by slightly increased particle size and EDS analysis of the PtSn(1:3)/Z-280 catalyst.

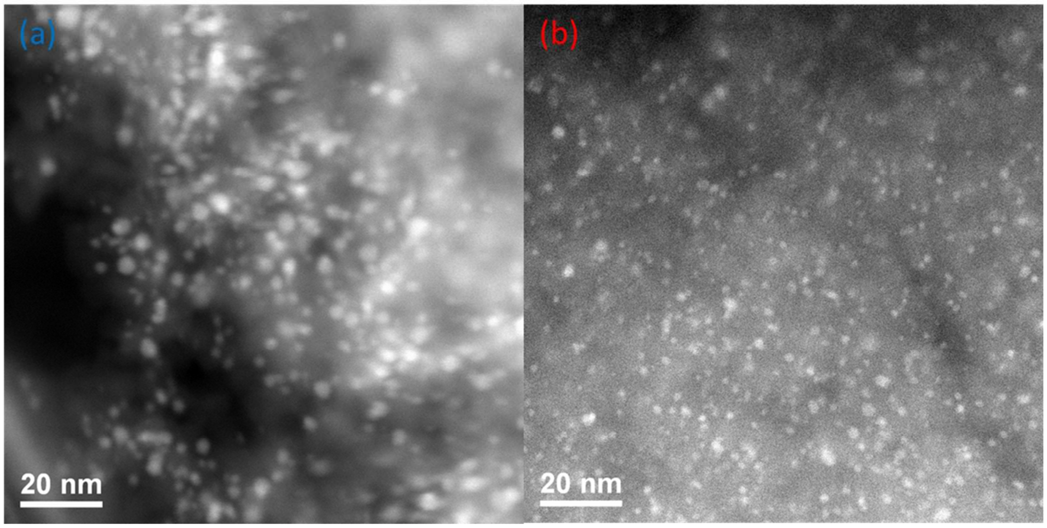

Figure 4. STEM images of (a) Pt/SiO_2, (b) Pt/H-ZSM-5 catalysts.

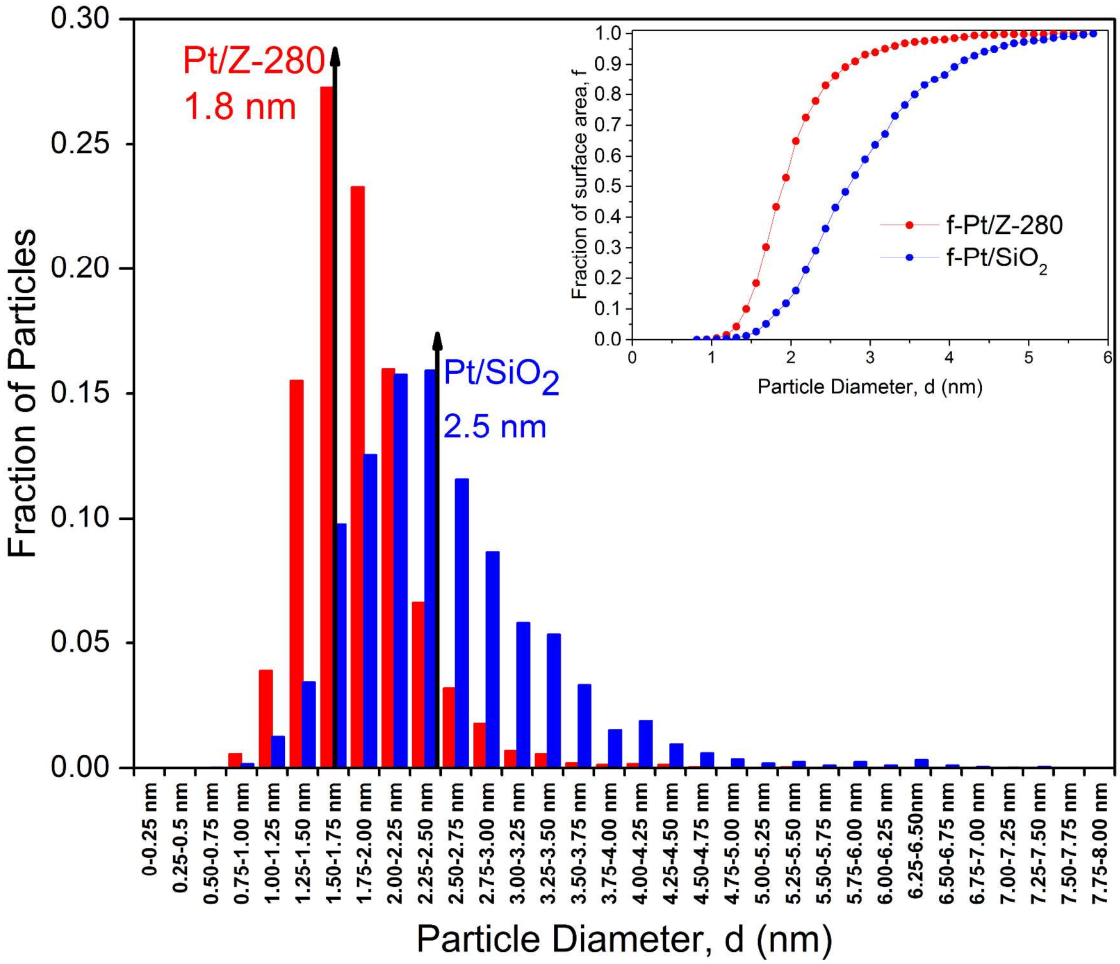

Figure 5. Particle size distribution of Pt/SiO_2 and Pt/Z-280. Inset displays the fraction of the total catalytic surface area as a function of particle size.

3.6 Effect of support acidity of the zeolite supported catalysts on catalytic activity: To study the effect of surface acidity on catalyst performance and the product distribution of zeolite-supported catalysts, we prepared PtSn(1:2) catalysts using more acidic H-ZSM-5 supports: Z-80, Z-50 and Z-23. Figure 6a shows the ethylene TOF as a function of time on stream over four PtSn(1:2) catalysts supported on H-ZSM-5 supports with different acidity. The highest rate of ethylene production was observed on the PtSn(1:2)/Z-50 catalyst. The catalyst showed an increasing ethylene TOF profile up to more than 20 h, after which it began to decrease. The less acidic catalyst PtSn(1:2)/Z-80 reached an earlier peak around 10 h with almost half of the ethylene TOF value of PtSn(1:2)/Z-50, and the least acidic PtSn(1:2)/Z-280 catalyst yielded almost a flat profile compared to the other three more acidic catalysts. To compare the activity of the catalysts towards formation of aromatics, the formation rates of benzene and naphthalene per mass of catalyst are plotted in Figure 6b and Figure 6c, respectively. The catalysts with the two most acidic supports, PtSn(1:2)/Z-23 and PtSn(1:2)/Z-50, showed the highest activity both for benzene and naphthalene production. The two less acidic catalysts, PtSn(1:2)/Z-80 and PtSn(1:2)/Z-280, were significantly less active for production of aromatics and deactivated during time on stream. On the PtSn(1:2)/Z-23 catalyst, the maximum formation rate was achieved at 15 h, and on the PtSn(1:2)/Z-50 it was achieved around 20 h. For both catalysts, these time points were earlier than the time for maximum production of ethylene. The initially increasing and then decreasing volcano-shaped activity profile for the formation of all the products suggests the formation of a reactive "hydrocarbon pool" on the acidic surface during the earlier period of reaction, similar to the hydrocarbon pool concept extensively studied and described in methanol-to-olefin (MTO) literature. It can be hypothesized that oligomerization of ethylene on the acid sites takes place together with interaction with the higher hydrocarbon structures of polyaromatics deposited in the pores.[42,43] After the maximum rate for ethylene formation is achieved, methane conversion is suppressed by deactivation.

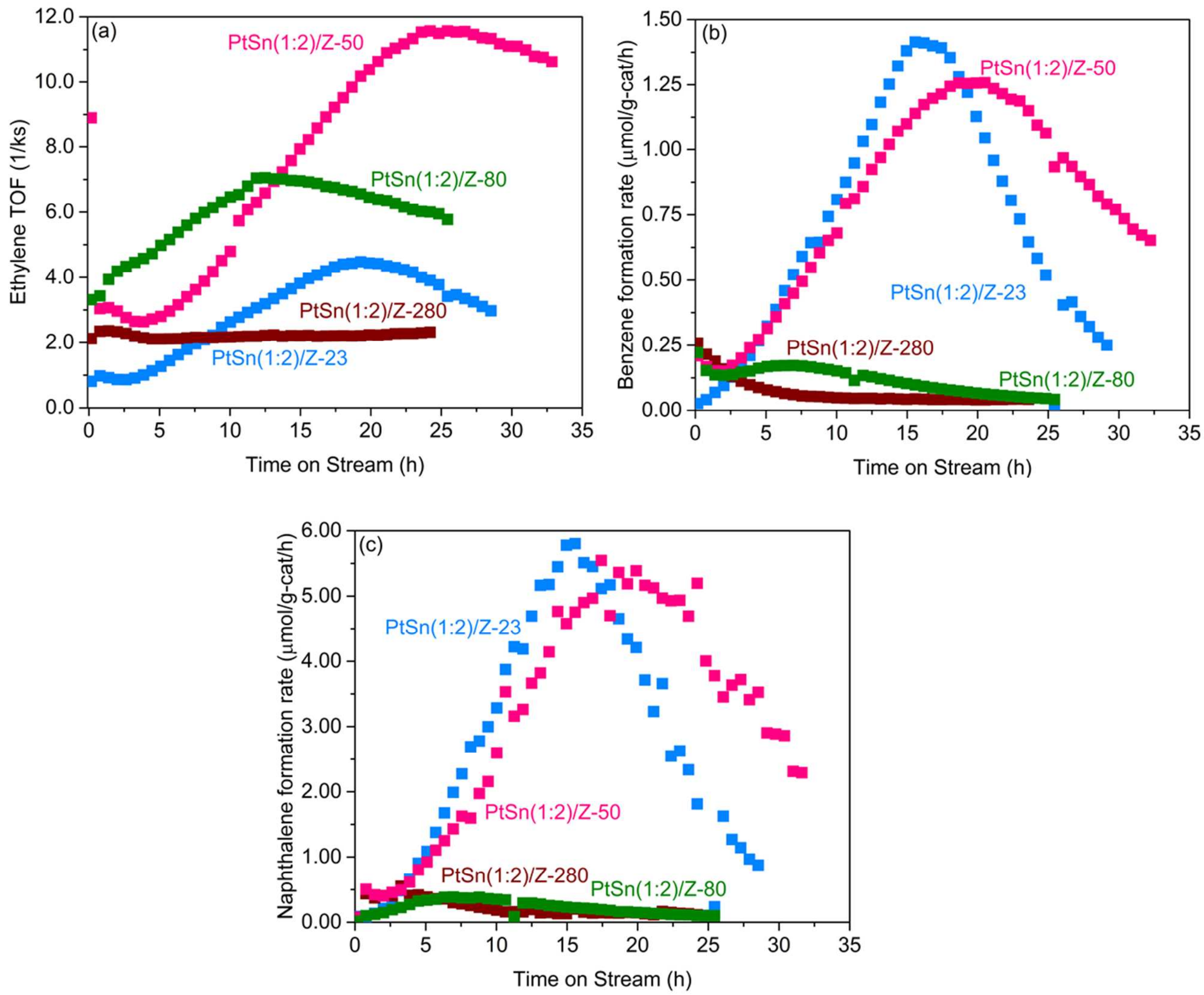

Figure 6. Effect of support acidity on (a) ethylene TOF (b) benzene formation rate and (c) naphthalene formation rate of zeolite-supported catalysts. *Conditions*: CH_4 flowrate = 10.5 cm^3(STP)/min, T = 973 K, catalyst mass = 0.25 g.

The methane conversion to detectable products (left axis) and the selectivities of the catalysts towards ethylene, ethane, benzene and naphthalene (right axis) over total hydrocarbon products excluding coke are plotted for each catalyst in Figure 7 a-d. The PtSn(1:2)/Z-50 catalyst showed the highest conversion, reaching approximately 0.30%, followed by the PtSn(1:2)/Z-23 catalyst. Conversion profiles of both catalysts were similar to the profiles for aromatics formation. The least acidic PtSn(1:2)/Z-280 catalyst had low conversion, as indicated by its low ethylene TOF and aromatic formation rates. On all the catalysts, regardless of their activity, ethylene was the product with highest selectivity, and benzene formation was significantly lower during the entire time on stream. Over the two most active catalysts, there were visibly opposite trends between ethylene and naphthalene selectivities. During the initial periods of the reaction while ethylene formation was still increasing, its selectivity decreased in the favor of naphthalene formation, which subsequently decreased when the ethylene selectivity began to increase again. The benzene selectivities of the catalysts were lower than naphthalene, supporting the argument that naphthalene was formed from benzene[44]. The delay in the maximum rate of ethylene formation compared to aromatics can be explained by faster oligomerization of ethylene to benzene on the more acidic catalysts, compared to desorption of ethylene from the catalyst. After the maximum rate is reached, the catalyst begins to deactivate due to coke deposition.

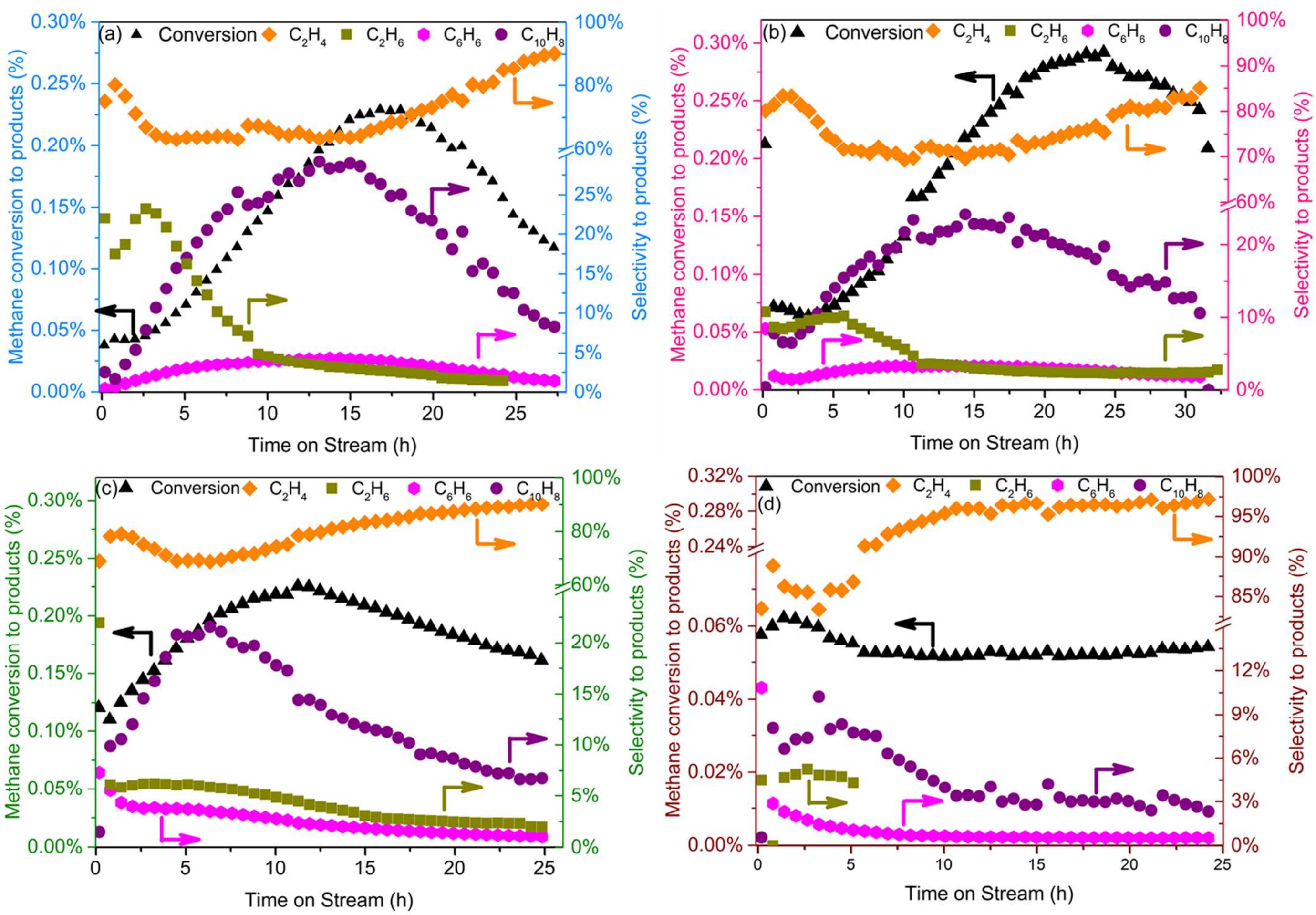

Figure 7. Effect of support acidity on methane conversion to detectable products and selectivities of (a) PtSn(1:2)/Z-23, (b) PtSn(1:2)/Z-50 (c) PtSn(1:2)/Z-80 and (d) PtSn(1:2)/Z-280. *Conditions*: CH_4 flowrate = 10.5 cm^3(STP)/min, T = 973 K, catalyst mass = 0.25 g.

As seen in Table 5, quantification of the amount of coke deposited on spent zeolite-supported catalysts showed that the catalysts supported on more acidic supports had higher extents of coke deposition, while the PtSn catalysts supported on the Z-280 support and the relatively inactive Pt/Z-280 catalyst had lower amounts of coke.

Table 5. Coke deposition on spent zeolite-supported catalysts

Catalyst	Carbon deposition by TGA (mmol/gcat)
Pt/Z-280	2.1
PtSn(1:3)/Z-280	3.6
PtSn(1:2)/Z-23	9.6
PtSn(1:2)/Z-50	8.9
PtSn(1:2)/Z-80	10
PtSn(1:2)/Z-280	6.5

In previously reported product formation rates, benzene was the main aromatic product, with selectivity higher than 60%.[3,12,18,19,28] However, for our catalysts with the two most acidic supports (Z-23 and Z-50), naphthalene was the major aromatic product, with formation rates up to 7 times higher than that of benzene. Over these two catalysts, when naphthalene formation reached its maximum rate, the selectivity to ethylene was 60%, naphthalene was 30%, and benzene was less than 5%. Furthermore, the total rate of carbon product formation (the sum of ethylene, benzene and naphthalene) on the PtSn(1:2)/Z-50 catalyst was approximately 2.5 mmol-C/mol-Pt.s, which is comparable to the calculated values of 0.1[45], 0.2[9], 0.3[17], 0.6[20], 0.7[19], 2.1[21], 9.2[24] and 15[16] mmol-C/(mol-Mo.s) from reported product formation rates for various Mo/H-ZSM-5 catalysts operated at 973 K and similar space velocities. In addition, we prepared Mo/H-ZSM-5 catalysts with 0.58 wt% and 4 wt% Mo, and we studied these catalysts for methane conversion at 973 K with 0.25 g of catalyst under 10.5 cm^3(STP)/min methane flow. The total rates of carbon product formation for these catalysts were 1.8 and 0.3 mmol-C/mol-Mo.s, respectively. To better illustrate this comparison, Figures 8 a-c display the rate of carbon product formation from ethylene, benzene and naphthalene on the 0.58 wt% Pt-Sn(1:2)/Z-50, 0.58 wt%

Mo/Z-50 and 4 wt% Mo/Z-50 catalysts. The total rate of carbon product formation on each catalyst is shown in Figure 8d. The rates in Figure 8 are normalized per Pt atom or per Mo atom in the catalyst.

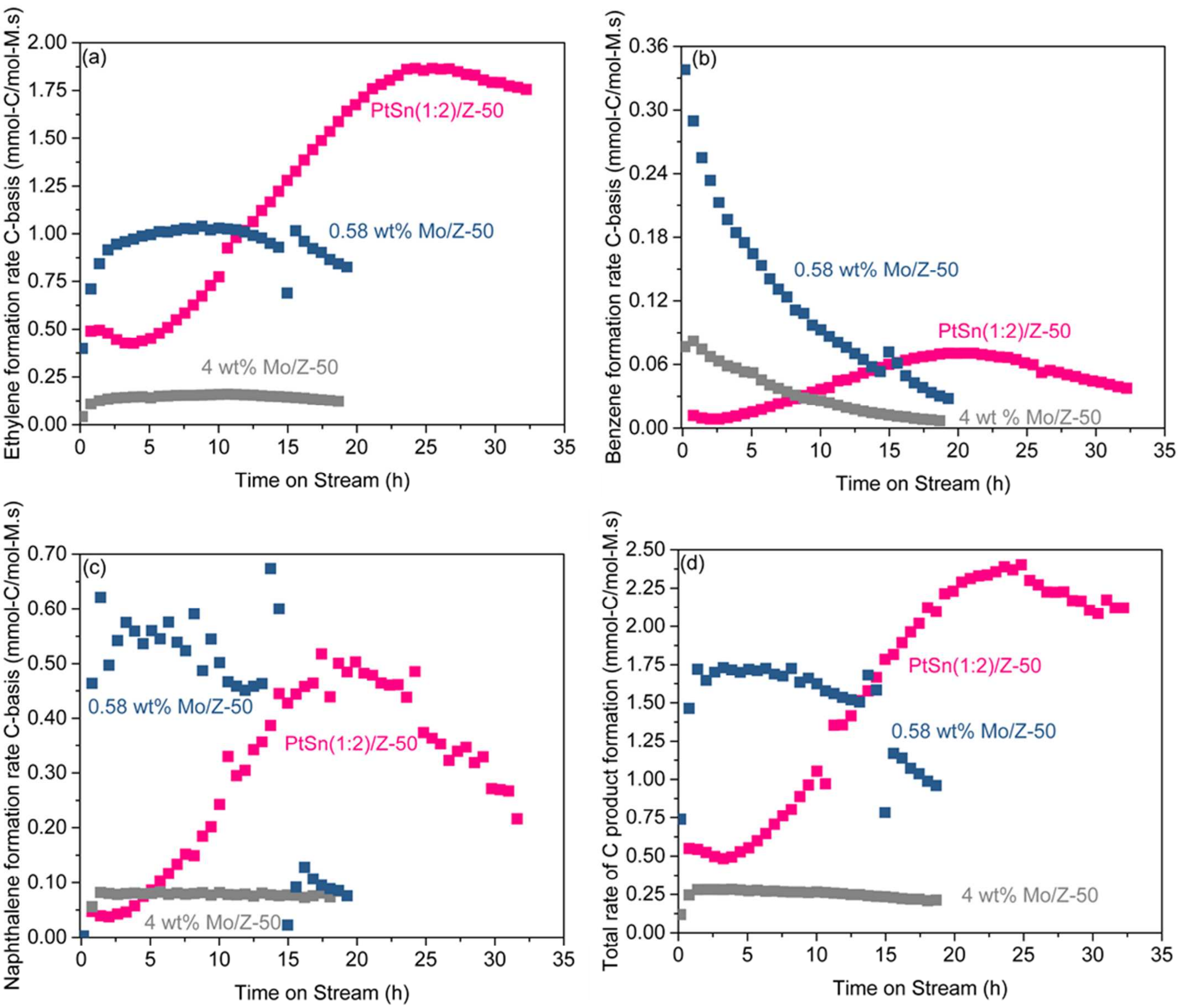

Figure 8. Rate of carbon product formation from (a) ethylene (b) benzene (c) naphthalene on the 0.58 wt% Pt-Sn(1:2)/Z-50, 0.58 wt% Mo/Z-50 and 4 wt% Mo/Z-50 catalysts. (d) Total rate of carbon product formation on each catalyst. *Conditions*: CH_4 flowrate = 10.5 cm^3(STP)/min, T = 973 K, catalyst mass = 0.25 g.

3.7. Microkinetic Model

A microkinetic model of methane conversion was developed to gain insight into catalyst reactivity by using DFT-derived parameters for terrace and stepped surfaces of Pt and Pt_3Sn. The Pt(433) terrace, Pt(433) step, Pt_3Sn(111) terrace and Pt_3Sn(211) step surfaces studied are shown in Figure 9. Details and key results of the model for the studied surfaces are given in the Supplementary Information. Without any adjustments in the DFT-derived parameters, the model was used to predict formation rates of the products and variations in surface coverages of the reaction intermediates under reaction conditions. The effect of Sn addition, H_2 co-feeding and particle size on the catalyst activity were investigated by comparing model predictions with experimental results.

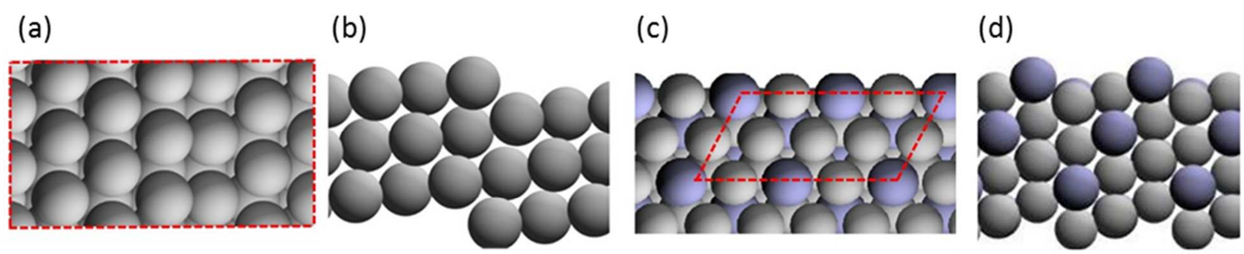

Figure 9. Model surfaces used in DFT calculations (a) Pt(433) terrace (b) Pt(433) step (c) Pt_3Sn(111) terrace and (d) Pt_3Sn(211) step. The unit cells of the terrace sites are highlighted.

The variation of the surface coverages of intermediates and ethylene TOF values of the studied surfaces are shown in Figure 10. The reversibilities (i.e., the ratio of the reverse rate to the forward rate) of the elementary steps carrying the reaction flux for the various surfaces predicted by microkinetic model are shown in Table 6.

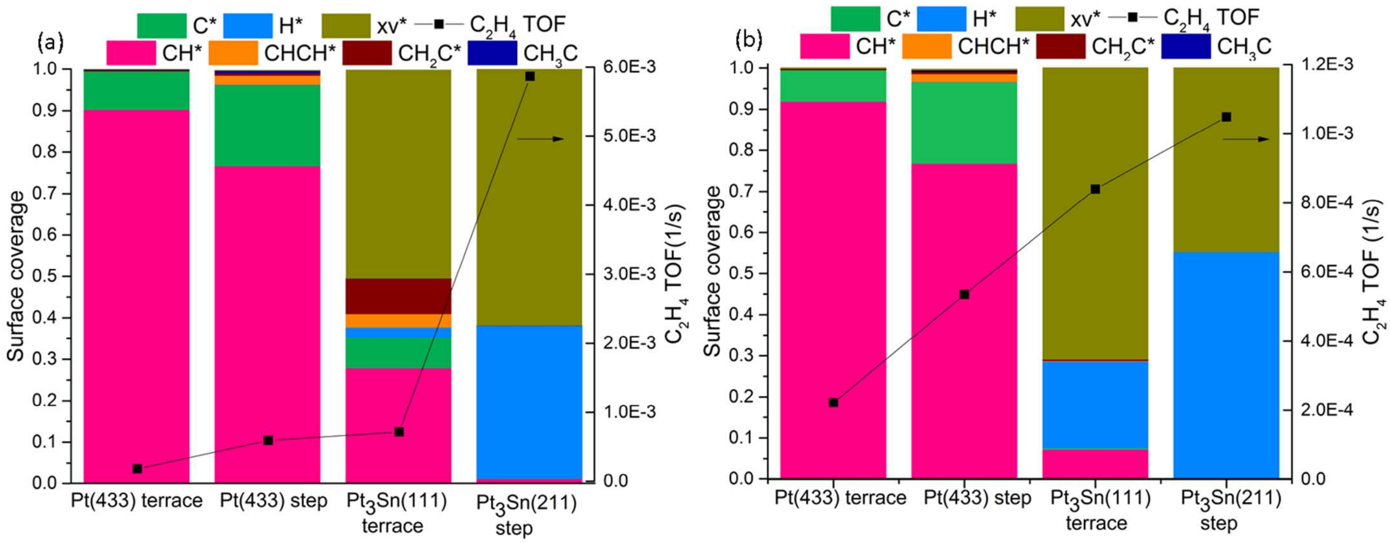

Figure 10: Surface coverages and ethylene TOF values of the studied surfaces predicted by the microkinetic model (a) no co-feeding conditions (b) 5% H_2 co-feeding with methane. (Experimental conditions same as Figure 1 and Figure 2) Left axis shows surface coverage of the indicated species, right axis shows the ethylene TOF values.

The model predicted that terrace and steps of Pt were almost fully covered with adsorbed CH* and C* fragments, with a slightly lower total coverage on Pt step sites, corresponding to a 2.4 times higher ethylene TOF. The elementary C-C coupling step with the highest rate was found as CH* + CH* → CHCH* which carried the 34% of the reaction flux on Pt terrace and 46% of the reaction flux on Pt step sites. On Pt terrace sites, the elementary step with the highest degree of rate control was the activation of adsorbed methane and desorption of the hydrogen, whereas on Pt steps, desorption of ethylene from the surface also had significant degrees of rate control.

Coverages of the surface by adsorbed CH* and C* were significantly lower on the $Pt_3Sn(111)$ terrace than on the Pt(111) terrace. On the $Pt_3Sn(111)$ terrace, the coverage of adsorbed CH* decreased to 0.28 from 0.92 and 0.77 on terrace and steps of Pt, and the coverage of adsorbed C* decreased to 0.07 from 0.09 and 0.2 on terrace and steps of Pt. Furthermore, 50% of the sites on the $Pt_3Sn(111)$ terrace were calculated to be vacant. The elementary C-C coupling step with the highest rate on the $Pt_3Sn(111)$ terrace was identified to be $CH_2* + C* \rightarrow CH_2C*$, which carried the 49% of the reaction flux, and similar to the Pt terrace, the adsorbed methane activation step possessed the highest degree of rate control for ethylene formation. Addition of Sn to the Pt terrace led to a 4 fold increase in ethylene TOF compared to the terrace of pristine Pt.

We also considered the reactivity of a stepped bimetallic surface, $Pt_3Sn(211)$. The microkinetic model predicted that the stepped surface was cleaner, with a fraction of vacant sites as 0.62. The predominant elementary C-C coupling step was $CH* + CH* \rightarrow CHCH*$. Similar to the other surfaces, activation of the adsorbed methane was the rate controlling step.

The model was also used to predict ethylene TOF values of the surfaces for 5% H_2 co-feed conditions. The coverage trends for the surfaces remained similar, i.e., the pristine Pt sites were not significantly influenced by H_2 co-feeding and again covered with adsorbed CH* and C* fragments, and both of the Pt_3Sn surfaces were calculated to have more than 40% vacant sites. A significant change upon co-feeding 5% H_2 was observed in the predictions for adsorbed H* coverage and fraction of vacant sites on Pt_3Sn surfaces. Specifically, values of H* coverage increased from 0.02 to 0.21 on $Pt_3Sn(111)$ terrace and increased from 0.03 to 0.21 on $Pt_3Sn(211)$ step.

Table 6: Reversibilities of elementary steps carrying the reaction flux on studied surfaces.

Elementary Step	Pt(433) terrace	Pt(433) step	$Pt_3Sn(111)$ terrace	$Pt_3Sn(211)$ step
Adsorption				
CH_4 + * <--> CH_4*	-	-	-	-
Dehydrogenation				
CH_4* + * <--> CH_3* + H*	0.18**	0.84**	0.01**	0.18**
CH_3* + * <--> CH_2* + H*	0.95	-	-	-
CH_2* + * <--> CH* + H*	-	-	-	-
CH* + * <--> C* + H*	-	-	-	-
C-C coupling				
CH* + C* <--> CHC* + *	-	-	-	0.77
CH* + CH* <--> CHCH* + *	-	-	-	0.77
CH_2* + CH* <--> CH_2CH* + *	-	-	-	0.77
Hydrogenation				
CHC* + H* <--> CH_2C* + *	-	-	-	-
CHC* + H* <--> C_2H_2* + *	-	-	-	-
CHCH* + H* <--> CH_2CH* + *	-	-	-	-
CH_2C* + H* <--> CH_2CH* + *	-	-	-	-
CH_2CH* + H* <--> CH_2CH_2* + *	0.83	-	-	0.52
Desorption				
CH_2CH_2* <--> CH_2CH_2 + *	0.61	0.62**	-	-
2H* <--> H_2 + 2*	0.01**	0.02**	-	-

(**) denotes elementary steps with significant degree of rate control, (-) denotes elementary steps with reversibilities approximately equal to unity.

As tabulated in Table 7, comparison of the ethylene TOF values predicted by the microkinetic model and experimental results showed that the model is able to capture the trends resulting from addition of Sn to the Pt, H_2 co-feeding of the catalyst, and the structure sensitivity of the reaction. In accordance with our experimental findings, the results from the microkinetic model predict that Pt_3Sn catalysts have higher ethylene TOF values than pristine Pt catalysts. The predicted increase in the rate upon addition of Sn is greater than the experimentally observed increase. The lower extent of bimetallic formation between Pt and Sn as evidenced by EDS analysis, might have caused the lower enhancement in the activity.

In the case of H_2 co-feeding, step sites of Pt and Pt_3Sn surfaces predicted the observed decrease in the ethylene TOF. Combining these results from the microkinetic model with the results from our experimental studies, we conclude that H_2 co-feeding on PtSn catalysts leads to a surface with a low coverage of hydrocarbon species, which decreases the ethylene TOF but also leads to decreased extent of coke deposition on the metal sites, thereby improving catalyst stability. In addition, step sites of both Pt and Pt_3Sn were predicted to have higher ethylene TOF values compared to their terrace site counterparts, reflecting the experimentally observed enhancement in switching from silica to zeolite supported catalysts.

Step sites of Pt_3Sn were predicted to be significantly more active due their cleaner surfaces (30 times higher ethylene TOF on $Pt_3Sn(211)$ step compared to the Pt step). Accordingly, the high activity predicted for the step sites supports the hypothesis that the high reactivity of PtSn/H-ZSM-5 catalysts may be related to these materials having a larger fraction of small nanoparticles, compared to SiO_2-supported catalysts, in agreement with the observation that Pt/H-ZSM-5 had up to 8 times higher fraction of total metal surface area compared to Pt/SiO_2 in the particle diameter range of 1-2 nm.

Table 7: Comparison of the ethylene TOF predictions from the model and experimental observations

Change	Surface	C_2H_4 TOF ratio (Model prediction)	C_2H_4 TOF ratio (Experimental)
Sn addition	terrace	3.9	2.7
($Pt/SiO_2 \rightarrow PtSn/SiO_2$)	step	9.9	2.7
Sn addition	terrace	1.5	4.7
(Pt/Z-280 → PtSn/Z-280)[a]	step	9.7	4.7
H_2 co-feeding	terrace	1.2	0.7
0 → 5% H_2 on Pt/SiO_2	step	0.9	0.7
H_2 co-feeding	terrace	1.2	0.4
0 → 5% H_2 on $PtSn/SiO_2$	step	0.2	0.4
Effect of particle size	Pt	3.2	9.9[c]
terrace → step[b]	PtSn	8.2	17.4[d]

[a]Predictions on the Z-280 supported catalysts were obtained by using Pt/Z-280 and Pt-Sn(1:3)/Z-280 catalyst site densities in the microkinetic model,
[b]Experimental value for representing the stepped surface was taken from [c]Pt/Z-280 and [d]Pt-Sn(1:3)/Z-280 catalysts

5. Conclusions

In this work, we show that Pt-based catalysts supported on SiO_2 and H-ZSM-5 can be employed in methane conversion under non-oxidative conditions. Adding Sn to Pt/SiO_2 results in a more active catalyst for ethylene formation. Treating the SiO_2-supported catalyst at 1123 K prior to reaction decreases the extent of coke formation. PtSn catalysts supported on H-ZSM-5 zeolite with (SiO_2:Al_2O_3 = 280) show higher ethylene TOF with improved carbon balance compared to SiO_2-supported catalysts. By varying the acidity of the support, a bifunctional catalyst can be obtained, resulting in a PtSn(1:2)/Z-XX catalyst (XX stands for SiO_2:Al_2O_3 = 23,50,80) which forms benzene with a higher rate by conversion of ethylene on acidic sites. PtSn catalysts supported on zeolites with SiO_2:Al_2O_3 = 23 and 50 produce significant amounts of naphthalene. The total rate of production of carbon in the observed products (i.e., the sum of ethylene + benzene + naphthalene) of the PtSn(1:2)/Z-50 catalyst is comparable with state-of-the-art Mo/H-ZSM-5 catalysts both reported in the literature and prepared in this study. Based on microkinetic model predictions and STEM imaging, the high activity of bimetallic H-ZSM-5 catalysts is suggested to be caused by the presence of the smaller metal nanoparticles (1-2 nm) on the zeolite-supported catalyst compared to the SiO_2-supported catalyst.

Corresponding Author

*E-mail : jdumesic@wisc.edu

Notes

The authors declare no competing financial interest.

Supporting Information: Development of microkinetic model, forward and reverse rate constants of the elementary steps used in the microkinetic model, surfaces studied by density functional theory. This material is available free of charge via the Internet at http://pubs.acs.org

Acknowledgements:

This work was financially supported by Air Force Office of Scientific Research under a Basic Research Initiative grant (AFOSR FA9550-16-1-0141). Computational resources at the DoD High Performance Computing Modernization Program (US Air Force Research Laboratory DoD Supercomputing Resource Center (AFRL DSRC), the US Army Engineer Research and Development Center (ERDC), and the Navy DoD Supercomputing Resource Center (Navy DSRC)) supported by the Department of Defense, were used to conduct this work. The authors acknowledge use of instrumentation supported by UW MRSEC (DMR-1121288) and the UW

NSEC (DMR-0832760). TGA studies were performed in UW-Madison Soft Materials Laboratory. The authors also acknowledge Madelyn R. Ball for collection of STEM data. A.H.M. acknowledges the support from Great Lakes Bioenergy Research Center (DOE Office of Science BER-DE-FC02-07ER64494). K.R.R.D. and J.B.M. acknowledge the support from the College of Engineering at the University of Wisconsin-Madison through the College's Research Innovation Committee. J.A.D acknowledges support by the U.S. Department of Energy, Office of Basic Energy Sciences (DE-SC0014058).

6. References

1- Xu, Y.; Lin, L. *Appl. Catal., A* **1999**, *188*, 53–67.

2- Karakaya, C.; Kee, R. J. *Prog. Energy Combust. Sci*. **2016**, *55*, 60–97.

3- Shu, Y.; Ichikawa, M. *Catal. Today* **2001**, *71*, 55–67.

4- Ma, S.; Guo, X.; Zhao, L.; Scott, S.; Bao, X. *J. Energy Chem.* **2013**, *22*, 1–20.

5- Shu, Y.; Ma, D.; Xu, L.; Yide, X.; Bao, X. *Catal. Lett.* **2000**, *70*, 67-73.

6- Wang, L.; Tao, L.; Xie, M.; Xu, G.; Huang, J.; Xu, Y. *Catal. Lett.* **1993**, *21*, 35–41.

7- Chen, L.; Lin, L. W; Xu, Z. S.; Li, X. S.; Zhang, T. *J. Catal.* **1995**, *157*, 190–200.

8- Wang, D.; Lunsford, J. H.; Rosynek, M. P. *Top. Catal*. **1996**, *3*, 289–297.

9- Solymosi, F.; Erdöhelyi, A.; Szöke, A. *Catal. Lett*. **1995**, *32*, 43–53.

10- Jiang, H.; Wang, L.; Cui, W.; Xu, Y. *Catal Lett*. **1999**, *57*, 95–102.

11- Solymosi, F.; Szöke, A.; Cserényi, J. *Catal. Lett.* **1996**, *39*, 157–161.

12- Derouane-Abd Hamid, S. B.; Anderson, J. R.; Schmidt, I.; Bouchy, C.; Jacobsen, C. J.; Derouane, E. G. *Catal. Today* **2000**, *63*, 461–469.

13- Mériaudeau, P.; Ha, V. T. T.; Tiep, L. Van *Catal. Lett.* **2000**, *64*, 49–51.

14- Liu, Z.; Nutt, M. A.; Iglesia, E. *Catal Lett.* **2002**, *81*, 271–279.

15- Kojima, R.; Kikuchi, S.; Ichikawa, M. *Chem. Lett.* **2004**, *33*, 1166-1167.

16- Shu, Y.; Ohnishi, R.; Ichikawa, M. *J. Catal.* **2002**, *206*, 134–142.

17- Ohnishi, R.; Liu, S.; Dong, Q.; Wang, L.; Ichikawa, M. *J. Catal.* **1999**, *182*, 92–103.

18- Lacheen, H. S.; Iglesia, E. *J. Catal.* **2005**, *230*, 173–185.

19- Xu, Y.; Song, Y.; Suzuki, Y.; Zhang, Z.-G. *Catal. Sci. Technol.* **2014**, *4*, 3644-3656.

20- Fila, V.; Bernauer, M.; Bernauer, B.; Sobalik, Z. *Catal. Today* **2015**, *256*, 269–275.

21- Burns, S.; Hargreaves, J. S. J.; Pal, P.; Parida, K. M.; Parija, S. *Catal. Today* **2006**, *114*, 383–387.

22- Wang, L.; Xu, Y.; Wong, S.-T.; Cui, W.; Guo, X. *Appl. Catal., A* **1997**, *152*, 173-182.

23- Wong, S.-T.; Xu, Y.; Wang, L.; Liu, S.; Li, G.; Xie, M.; Guo, X. *Catal. Lett.* **1996**, *38*, 39–43.

24- Shu, Y.; Xu, Y.; Wong, S.-T.; Wang, L.; Guo, X. *J. Catal.* **1997**, *170*, 11–19.

25- Sily, P. D.; Noronha, F. B; Passos, F. B. *J. Nat. Gas Chem.* **2006**, *15*, 82–86.

26- Weckhuysen, B. M.; Rosynek, M. P.; Lunsford, J. H. *Catal. Lett.* **1998**, *52*, 31–36.

27- Liu, H.; Li, T.; Tian, B.; Xu, Y. *Appl. Catal., A* **2001**, *213*, 103-112.

28- Song, Y.; Xu, Y.; Suzuki, Y.; Nakagome, H.; Zhang, Z.-G. *Appl. Catal., A* **2014**, *482*, 387-396.

29- Weckhuysen, B. M.; Wang, D.; Rosynek, M. P.; Lunsford, J. H. *Angew. Chem. Int. Ed.* **1997**, *36*, 2374-2376.

30- Wang, L.; Ohnishi, R.; Ichikawa, M. *J. Catal.* **2000**, *190*, 276–283.

31- Weckhuysen, B. M.; Wang, D.; Rosynek, M. P.; Lunsford, J. H. *J. Catal.* **1998**, *175*, 338–346.

32- Guo, X.; Fang, G.; Li, G.; Ma, H.; Fan, H.; Yu, L.; Ma, C.; Wu, X.; Deng, D.; Wei, M.; Tan, D.; Si, R.; Zhang, S.; Li, J.; Sun, L.; Tang, Z.; Pan, X.; Bao, X. *Science* **2014**, *344*, 616–619.

33- Belgued, M.; Pareja, P.; Amariglio, A.; Amariglio, H. *Nature* **1991**, 789–790.

34- Mielczarski, E.; Monteverdi, S.; Amariglio, A.; Amariglio, H. *Appl. Catal., A* **1993**, *104*, 215–228.

35- Xu, Y.; Liu, S.; Guo, X.; Wang, L.; Xie, M. *Catal. Lett.* **1995**, *30*, 135–149.

36- Chen, L.; Lin, L.; Xu, Z.; Zhang, T.; Li, X. *Catal. Lett.* **1996**, *39*, 169–172.

37- Pinglian, T.; Zhusheng, X.; Tao, Z.; Liayuan, C.; Liwu, L. *React. Kinet. Catal. Lett.* **1997**, *61*, 391–396.

38- Tshabalala, T. E.; Coville, N. J.; Scurrell, M. S. *Appl. Catal., A* **2014**, *485*, 238–244.

39- Tshabalala, T. E.; Coville, N. J.; Anderson, J. A.; Scurrell, M. S. *Appl. Catal., A* **2015**, *503*, 218–226.

40- Kappenstein, C.; Gue´rin, M.; Lázár, K.; Matusek, K.; Paál, Z. *J. Chem. Soc. Faraday Trans.* **1998**, *94*, 2463–2473.

41- Tessonnier, J.-P.; Louis, B.; Rigolet, S.; Ledoux, M. J.; Pham-Huu, C. *Appl. Catal. A Gen.* **2008**, *336*, 79–88.

42- Haw, J. F.; Song, W.; Marcus, D. M.; Nicholas, J. B. *Acc. Chem. Res.* **2003,** *34*, 317-326.

43- White, J. L. *Catal. Sci. Technol.* **2011**, *1*, 1630-1635.

44- Carlson, T.R.; Jae, J.; Huber, G.W. *ChemCatChem* **2009**, *1*, 107-110.

45- Liu, S.; Dong, Q.; Ohnishi, R.; Ichikawa, M. *Chem. Commun.* **1998**, 1217–1218.

46- Kresse, G.; Furthmuller, J. *Phys. Rev. B* **1996**, *54*, 11169-11186.

47- Kresse, G.; Furthmuller, J. *Comput. Mater. Sci.* **1996**, *6*, 15-50.

48- Blochl, P. E. *Phys. Rev. B* **1994**, *50*, 17953-17979.

49- Kresse, G.; Joubert, D. *Phys. Rev. B* **1999**, *59*, 1758-1775.

50- Perdew, J. P.; Wang, Y. *Phys. Rev. B* **1992**, *45*, 13244-13249.

Table of Contents Graphic

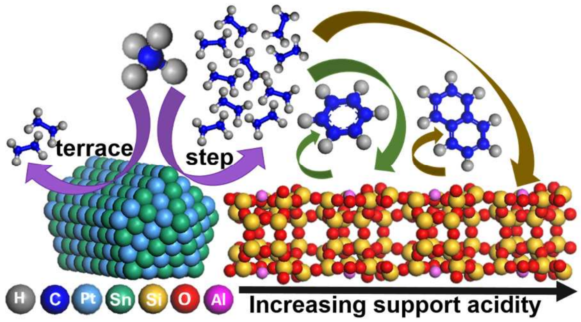

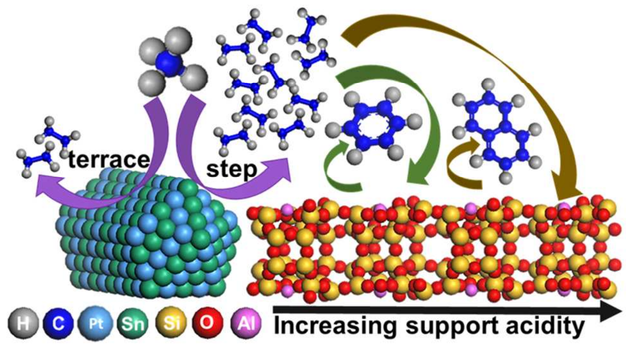

Graphical abstract

338x190mm (96 x 96 DPI)

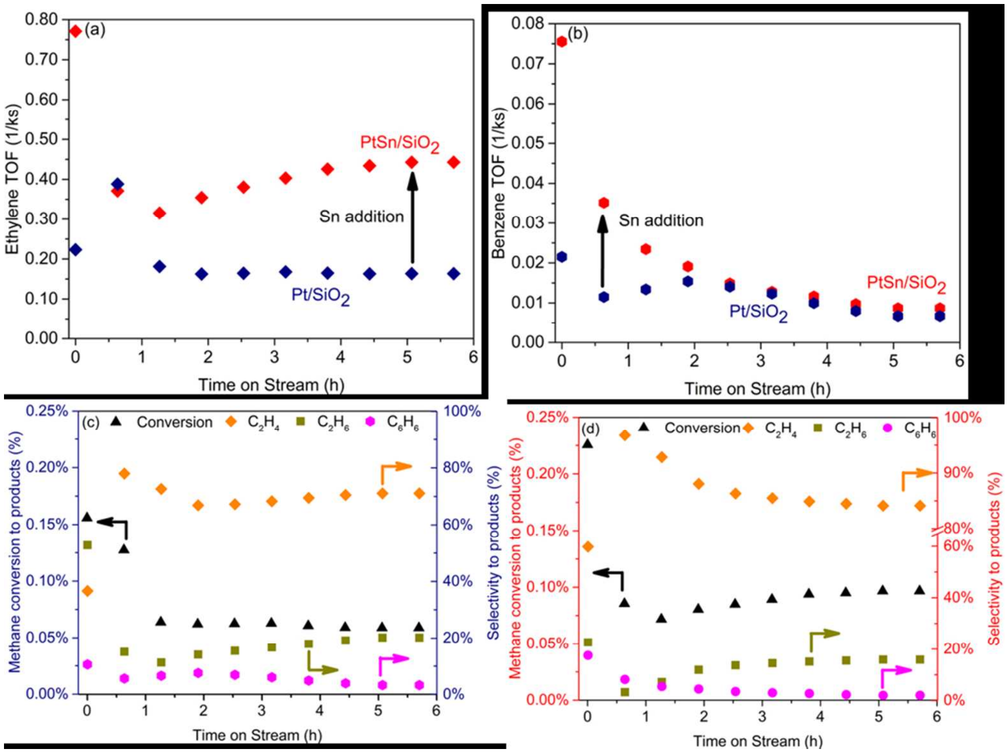

Figure 1

171x127mm (150 x 150 DPI)

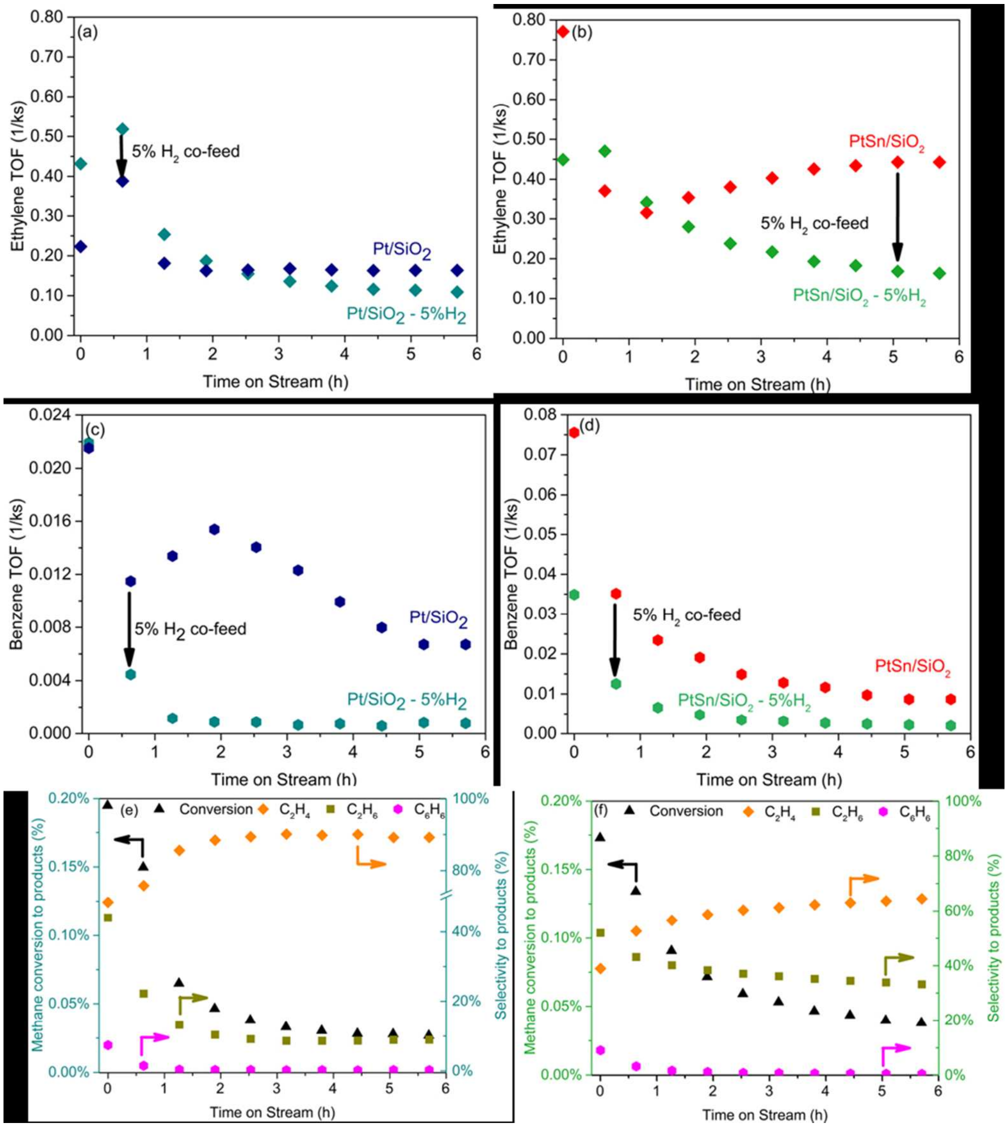

Figure 2

169x189mm (150 x 150 DPI)

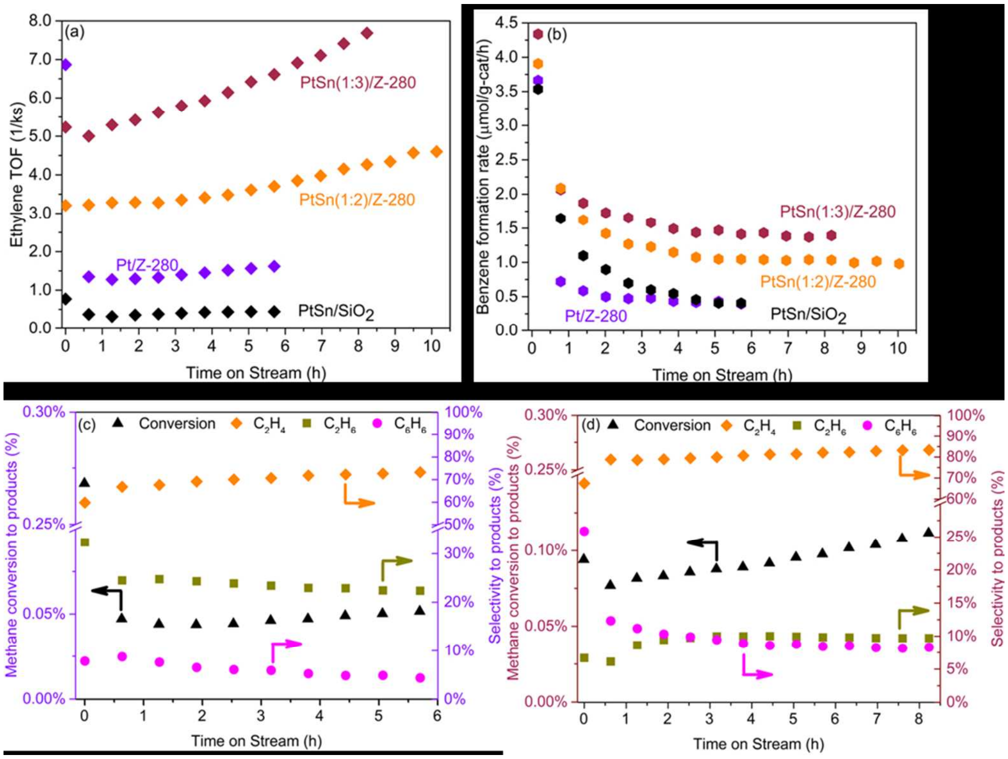

Figure 3

178x134mm (150 x 150 DPI)

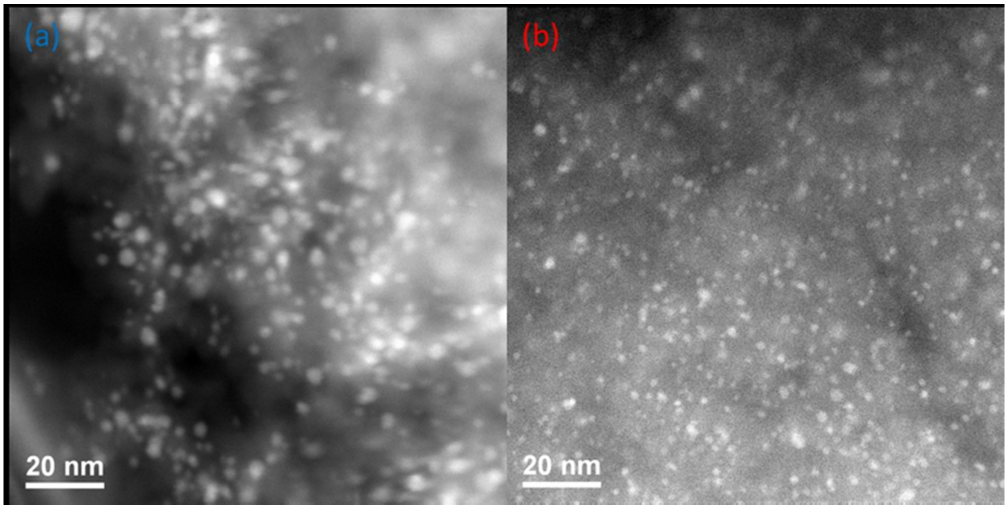

Figure 4

138x69mm (150 x 150 DPI)

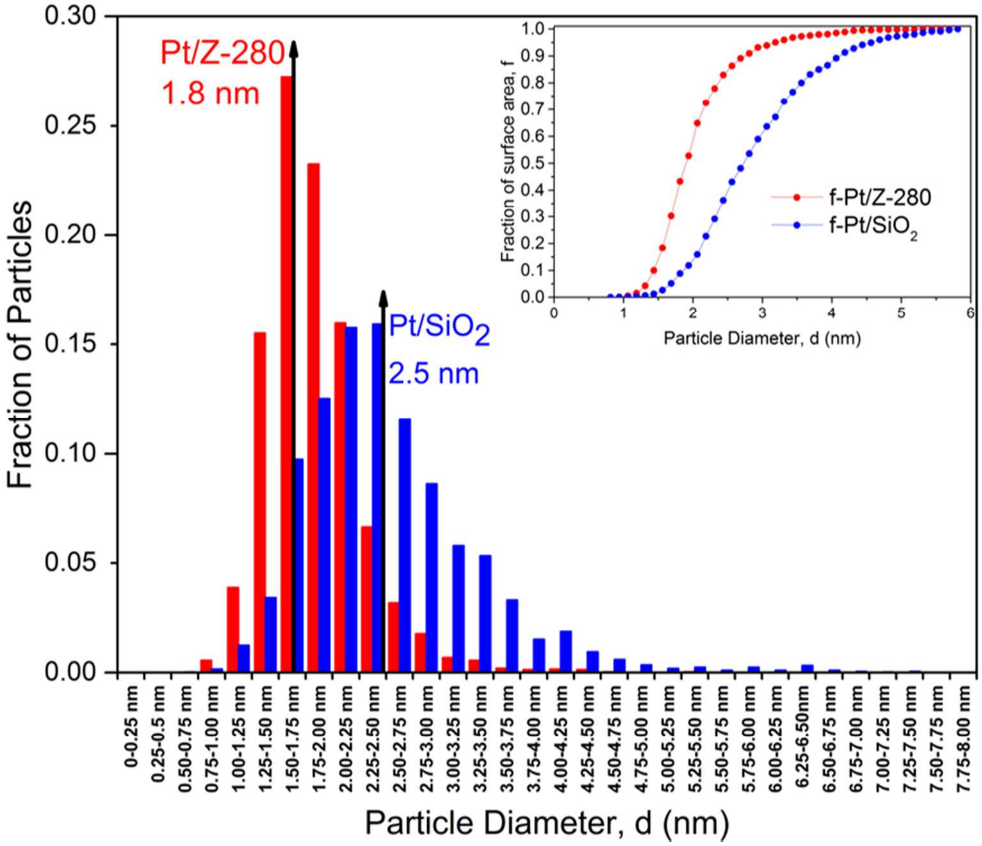

Figure 5

150x127mm (150 x 150 DPI)

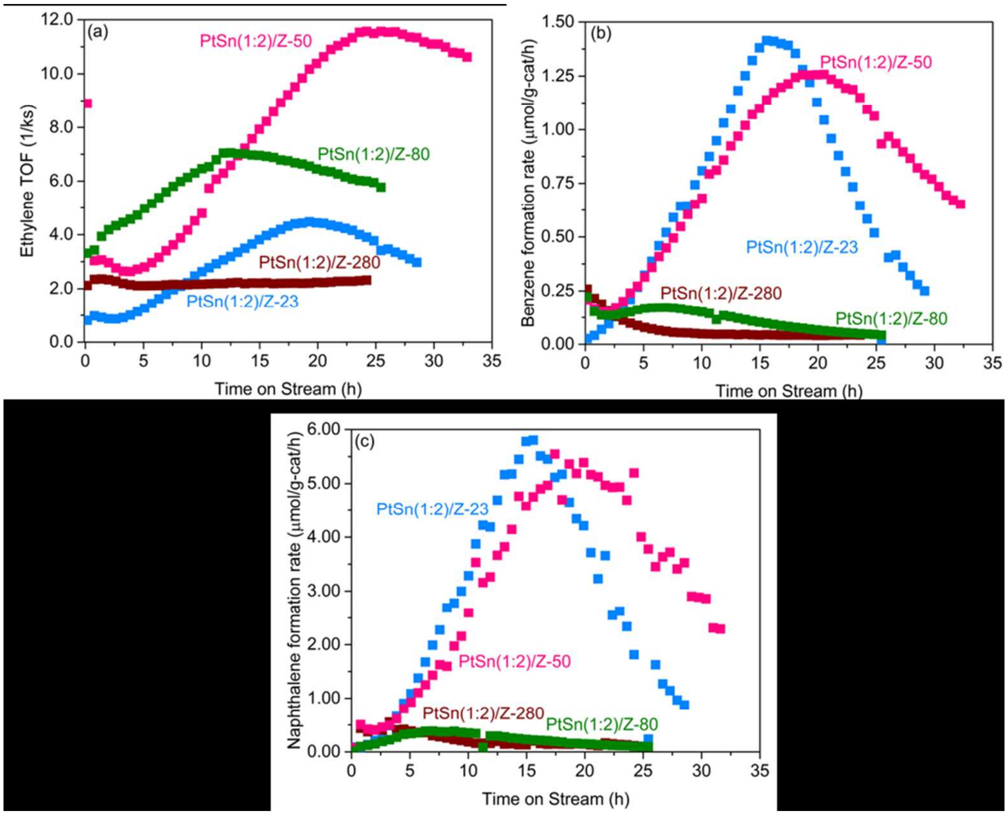

Figure 6

170x137mm (150 x 150 DPI)

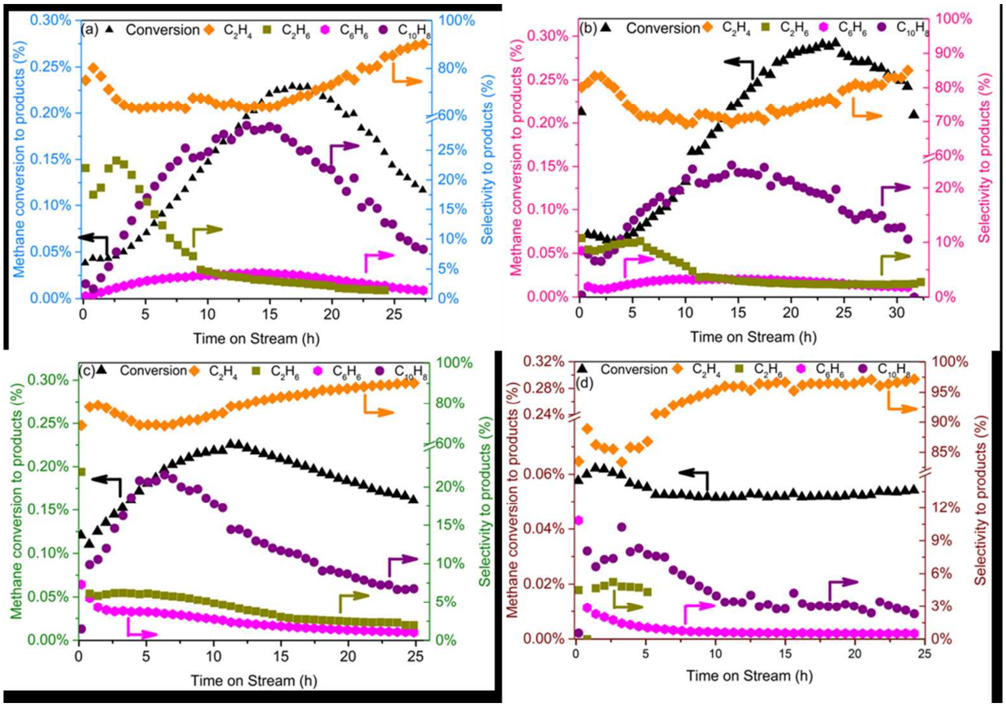

Figure 7

184x128mm (150 x 150 DPI)

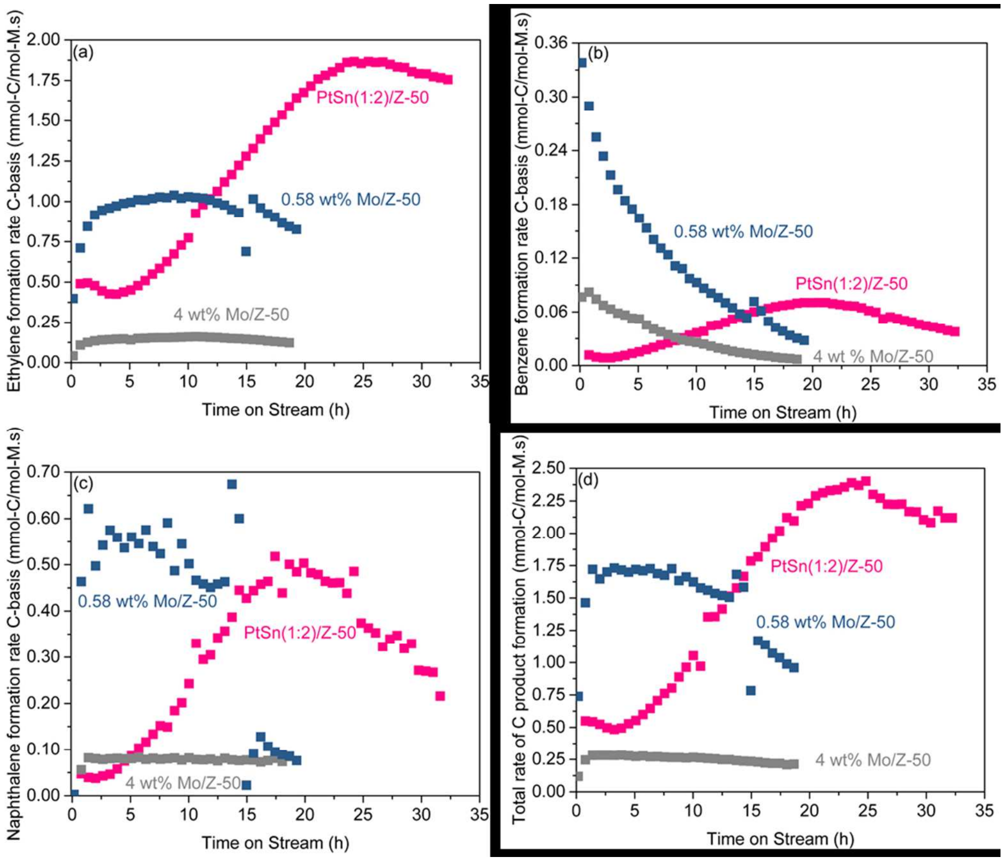

Figure 8

181x154mm (150 x 150 DPI)

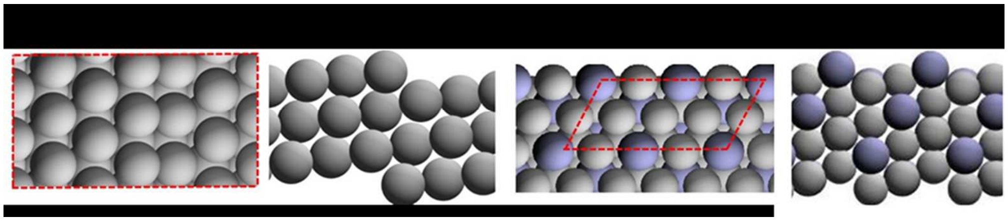

Figure 9

164x35mm (150 x 150 DPI)

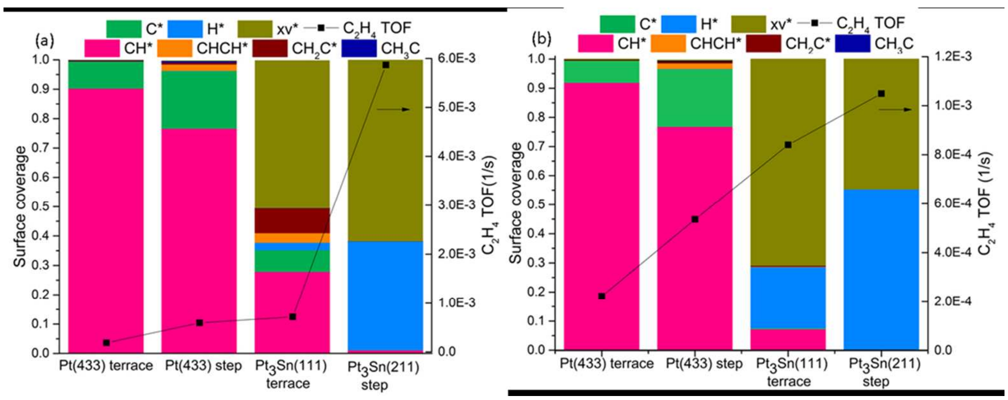

Figure 10

185x72mm (150 x 150 DPI)